Journal of Materials Chemistry A

ROYAL SOCIETY OF CHEMISTRY

REVIEW

View Article Online
View Journal | View Issue

Cite this: J. Mater. Chem. A, 2020, 8, 1511

Advances and challenges in electrochemical CO_2 reduction processes: an engineering and design perspective looking beyond new catalyst materials

Sahil Garg,[a] Mengran Li, *[a] Adam Z. Weber, [b] Lei Ge, [ac] Liye Li,[d] Victor Rudolph,[a] Guoxiong Wang[a] and Thomas E. Rufford *[a]

Received 26th September 2019
Accepted 12th December 2019

DOI: 10.1039/c9ta13298h

rsc.li/materials-a

Electrochemical CO_2 reduction (CO_2R) is one of several promising strategies to mitigate CO_2 emissions. Electrochemical processes operate at mild conditions, can be tuned to selective products, allow modular design, and provide opportunities to integrate renewable electricity with CO_2 reduction in carbon-intensive manufacturing industries such as iron and steel making. In recent years, significant advances have been achieved in the development of highly efficient and selective electrocatalysts for CO_2R. However, to realize fully the potential benefits of new electrocatalysts in low cost, large scale CO_2R electrolyzers requires advances in design and engineering of the CO_2R process. In this review, we examine the state-of-the-art in electrochemical CO_2R technologies, and highlight how the efficiency of CO_2R processes can be improved through (i) electrolyzer configuration, (ii) electrode structure, (iii) electrolyte selection, (iv) pH control, and (v) the electrolyzer's operating pressure and temperature. Although a comprehensive review of catalytic materials is beyond this review's scope, we illustrate how other engineering and design decisions may also influence CO_2R reaction pathways because of effects on mass transfer rates, the electrode surface chemistry, interactions with intermediate reaction species, and rates of charge transfer.

1 Introduction

Utilization of CO_2 from industrial waste gases is considered a complementary route to other CO_2 emission reduction strategies such as renewable energy sources, CO_2 capture and storage (CCS), and other low carbon emission technologies.[1] The main pathways to utilize CO_2 include reuse of CO_2 without

[a]School of Chemical Engineering, The University of Queensland, St Lucia 4072, Australia. E-mail: m.li6@uq.edu.au; t.rufford@uq.edu.au

[b]Joint Center for Artificial Photosynthesis, Lawrence Berkeley National Laboratory, 1 Cyclotron Rd, Berkeley, CA 94720, USA

[c]Center for Future Materials, University of Southern Queensland, Springfield 4300, Australia

[d]HBIS Group Technology Research Institute, Shijiazhuang, 050023, China

Sahil Garg is a PhD student in the School of Chemical Engineering at the University of Queensland, Australia investigating the interactions between electrolytes and catalysts for CO_2 reduction. Sahil received his B. Technology degree in Chemical Engineering from the Indian Institute of Technology Gandhinagar (IITGN), India in 2012, and a Masters in in Chemical Engineering from Universiti Teknologi PETRONAS, Malaysia in 2016. In September 2019, Sahil was named a Rising Star in the field of chemical engineering and materials by The Australian newspaper.

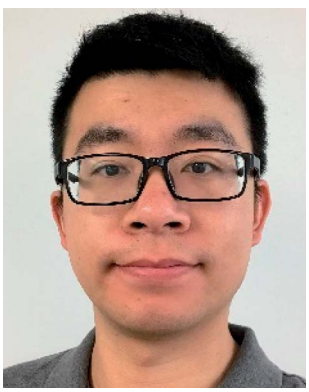

Mengran Li is a postdoctoral research fellow in the School of Chemical Engineering and UQ-HBIS Innovation Centre for Sustainable Steel at the University of Queensland, Australia. Mengran completed his Bachelor of Engineering in Chemical Engineering at Tianjin University, China (2008), and PhD from the University of Queensland in Australia (2012) for a thesis on cathode materials for solid oxide fuel cells. His current research focuses on development of transition metal-based material and electrochemical process for energy conversion and carbon mitigation.

conversion (*e.g.* enhanced oil recovery, supercritical CO_2)[2,3] or to convert the CO_2 to a valuable fuel, energy storage vector, or chemical feedstock. Among CO_2 conversion technologies such as biochemical, photosynthetic, thermo-catalytic, and photocatalytic processes,[4–7] electrochemical CO_2 reduction (CO_2R) is one of the most promising CO_2 utilization strategies because of the mild electrolyzer operating conditions, opportunities to tune the process towards desired products, the potential to use industrial or municipal wastewaters as electrolytes, and modular reactor designs.[8] In addition, CO_2R technologies could be integrated with renewable electricity generation from solar or wind[9–11] (as shown in Fig. 1) to reduce carbon footprints in carbon intensive manufacturing industries such as ammonia production or iron and steel production through CO recycling,[12] for example.

Table 1 shows several organisations report electrochemical CO_2R technologies to operate at pilot-scale with current densities in the range j = 100–200 mA cm^{-2}. These technologies could lead to commercially viable processes to convert CO_2 to CO,[13] light hydrocarbons including CH_4 and C_2H_4,[14] alcohols,[15] and chemical feedstocks like formic acid (HCOOH).[16] However, most of these technologies are currently too costly for practical applications and market penetration. The first challenge to low cost CO_2R is the high energy requirement to break bonds in the CO_2 molecule.[17] The second challenge is to achieve a high selectivity of CO_2 to desired products to minimize costs and complexity of product separation processes. Achieving high selectivity is difficult because a large number of CO_2R reactions and the competing hydrogen evolution reaction (HER) all have standard potentials (E^o) in a narrow range (−0.25 V to 0.17 V *vs.* standard hydrogen electrode (SHE)) as shown in Fig. 2. The

Adam Z. Weber is a staff scientist and Group Leader of the Energy Conversion Group at Lawrence Berkeley National Laboratory, USA. Adam holds B.S. and M.S. degrees from Tufts University, and a Ph.D. in chemical engineering from the University of California, Berkeley. He has authored over 100 peer-reviewed articles and 10 book chapters on fuel cells, flow batteries, and related electrochemical devices. Adam's work has been recognized by a number of awards including a a 2012 Presidential Early Career Award for Scientists and Engineers (PECASE), the 2014 Charles W. Tobias Young Investigator Award of the Electrochemical Society, and the 2016 Sir William Grove Award of the International Association for Hydrogen Energy.

Lei Ge is a research fellow in the Centre for Future Materials at the University of Southern Queensland, and an adjunct fellow in the School of Chemical Engineering at the University of Queensland, Australia. He completed his PhD in 2013 at the University of Queensland and ME in 2008 at the Nanjing University of Technology, China. His research interests includes materials for membrane separation and selective gas adsorption, metal organic frameworks related materials for electrolysis, and energy devices (e.g. fuel cells).

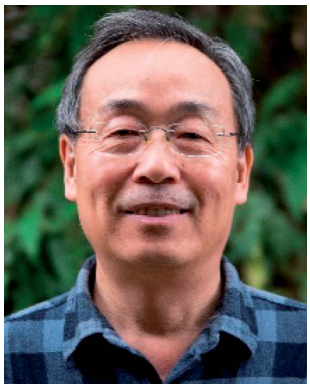

Guoxiong (Geoff) Wang is a Professor in Chemical Engineering at the University of Queensland, Australia. Geoff received his BEng in 1983, MEng in 1986, and PhD in 1990 from Northeastern University, China and specialized in process metallurgy focusing on iron- and steel-making. He joined the University of Queensland in 1996 and leads research on modeling and simulation of the Chemical and Metallurgical Engineering processes, coalbed methane (CBM) extraction and carbon dioxide geo-sequestration with enhanced coalbed methane (CO2-ECBM) recovery. His research activity and interests are directed towards developing energy and environmental technologies.

Thomas (Tom) Rufford is an Associate Professor in the School of Chemical Engineering at the University of Queensland, Australia. Tom completed his Bachelor and PhD degrees in Chemical Engineering at the University of Queensland in 2000 and 2009, respectively, with four years engineering practice in the oil industry between these degrees. His research interests include electrode materials for supercapacitors and electrocatalysts for CO_2 reduction, industrial gas separation and purification technologies, and fluid–solid interactions in coal bed methane production systems. Tom has published more than 65 journal articles, 2 book chapters, and an edited book on carbon materials.

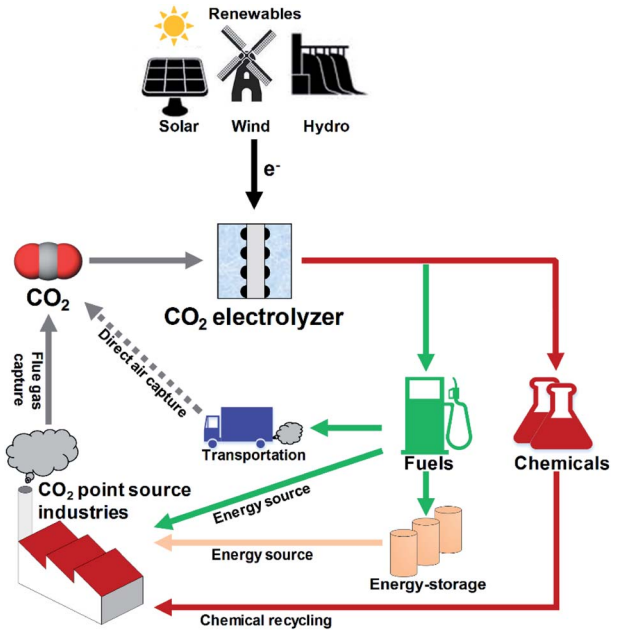

Fig. 1 Closing the carbon cycle. CO_2 electrolyzer utilizing renewable energy can convert the captured CO_2 into chemicals or fuels for direct usage or energy storage.

third challenge is to ensure the overall rate of reaction is not limited by rates of CO_2 mass transfer from the gas phase to electrolyte and to active sites on the cathode catalyst. The fourth practical challenge is to maintain stable electrocatalyst performance over extended operating periods because the catalyst can be poisoned by impurities in the electrolytes[18,19] or CO_2 feed gas (*e.g.* sulphur compounds), or by products stemming from corrosion of the electrolyzer components.[20–26]

To circumvent these challenges, a significant amount of research effort aims to develop highly efficient, stable, and selective CO_2R electrocatalysts. Many comprehensive reviews on CO_2R catalysts are available,[28–38] and these reviews cover advances in transition metals, alloys, metal–organic complexes, metal chalcogenides, metal–nitrogen–carbon materials, and carbon materials. Further review of electrocatalysts is beyond the scope of this article. Instead, we complement existing catalyst reviews with a critical analysis of engineering factors that affect the performance of CO_2R electrolyzers. These factors include the reactor configuration, electrode structures, electrolyte selection, and the choice of reaction conditions such as pH, pressure, and temperature. These engineering factors not only predetermine the CO_2R mass-transport characteristics but can also have significant impacts on the catalytic reaction pathways.[39–41] The review concludes with a discussion of the priorities for future research to understand better the fundamental mechanisms of CO_2R and improve CO_2R performance.

2 Working principles of electrochemical CO_2 reduction

A typical CO_2 electrolyzer (see for example Fig. 3a showing a H-cell type reactor used in research laboratories) consists of a cathode to reduce CO_2 to products such as CO or HCOOH/$HCOO^-$ and produce hydroxyl ions (OH^-); an anode to oxidize water *via* the oxygen evolution reaction (OER) that consumes OH^- or generates protons (H^+) and electrons (e^-); an electrolyte to conduct ions and to dissolve and transport CO_2 to the cathode active sites; an ion-exchange membrane or porous diaphragm to separate the cathode and anode electrodes; and a voltage source with sufficient potential (E) to transfer electrons from anode to cathode. In such a system, there are several key steps involved in a CO_2R process, including (1) mass transfer of CO_2 from the gas phase to the bulk electrolyte, (2) transport of dissolved CO_2 from the bulk electrolyte to cathode/electrolyte interface, (3) absorption of CO_2 at the cathode surface, (4) dissociation of adsorbed CO_2 species into adsorbed intermediates such as *COOH, *CO, *CHO, and *COH, (5) electron transfer from the cathode catalyst to intermediates, (6) desorption of products from the electrode, and (7) migration of products away from the cathode/electrolyte interface to the bulk gas or liquid phases.[48]

We start our discussion at the electron transfer step (5) to examine the minimum theoretical energy requirement for CO_2R. The minimum potential required for a CO_2R reaction is the half-cell standard potential described by $E^o = -\Delta G^0/nF$, where ΔG^0 is the Gibbs free energy at 1 atm and 298 K, n is the number of moles of electrons transferred in the half-cell reaction, and F is Faraday constant (96 485C mol^{-1}). For example, the half-cell reaction $CO_2(g) + 2H^+(aq.) + 2e^- \rightarrow CO(g) + H_2O(l)$ with $\Delta G^0 = 20.09$ kJ mol^{-1} has $E^\circ = -0.104$ V *vs.* SHE.[49] Other half-cell standard potentials at 1 atm and 298 K are shown in Fig. 2. To drive a sufficient CO_2R rate, an excess voltage or overpotential to E° must be applied to overcome the sum (R_{total}) of several energy barriers or resistances as described in eqn (1):

$$R_{total} = R_{cathode} + R_{anode} + R_{ions} + R_{membrane} + R_{bubble,cathode} + R_{bubble,anode} + R \quad (1)$$

The resistances include (1) the activation barriers or activation overpotentials (η_s)[50] for CO_2R at cathode ($R_{cathode}$) and OER at the anode (R_{anode}); (2) ohmic losses from conduction of ions (R_{ions}) in the bulk electrolytes, ion transport across the membrane ($R_{membrane}$); (3) loss of active electrode area from the bubbles formation at the electrodes (*e.g.* $R_{bubble,cathode}$ for CO and H_2 at the cathode, and $R_{bubble,anode}$ for O_2 at the anode);[51,52] and (4) the sum (R) of electrical resistances in other cell components and contact resistances between components.

Because the CO_2R reaction depletes CO_2 concentrations at the electrode surface, at high current densities the overall reaction rate can be limited by the rates of CO_2 mass-transfer to the electrode surface.[53] In addition according to the Nernst equation, the change in concentration affects the equilibrium potential and this effect can be approximated by the concentration overpotential.[49] In large scale industrial electrolyzers operating at high temperature concentration overpotential becomes important because at higher temperatures the activation overpotential is lower and the improved electrolyte conductivity leads to smaller ohmic losses.[54] Therefore, now that we have established the minimum energy requirements for

Table 1 Summary of lab-scale or soon to be commercially available electrochemical CO_2 reduction technologies[a]

Technology (location)	Throughput/scale	Reactor configuration	Catalysts	Electrolyte	Target Products	Notes	Reference
Opus-12 (Berkeley, USA)	Lab-scale	Proton exchange membrane (PEM) type electrolyzer	Anode: IrO_2, cathode: Ag nanoparticles supported on carbon foam[42]	Water	CO and O_2	Announced plans to develop renewable electricity operated CO_2R to ethylene, ethanol	13
Dioxide materials (Boca Raton, USA)	Lab-scale	Sandwich-type CO_2 electrolyzer where cathode and anode catalysts are painted on either side of the membrane	Anode: IrO_2 or RuO_2, cathode: carbon paper coated with silver/ionomer mixture[43]	10 mM $KHCO_3$ as anolyte and humidified CO_2 as catholyte[43]	>95% selectivity to CO[43]	Report 6 months stable catalyst operation	44
Carbon electrocatalytic recycling Toronto (CERT) (Toronto, Canada)	Lab-scale/pilot-scale cell	Flow cell modified from state-of-the-art fuel cells	Anode: made from cheap and conventional abundant earth metals, cathode: nanostructured metals based on copper[45]	7 M KOH[45]	70% selectivity for C_2H_4 (ref. 45)	Uniform selectivity for the initial 150 hours	14
Mantra energy alternatives Ltd (Vancouver, Canada)	100 kg per day pilot plant	Fuel-cell type CO_2 electrolyzer	*Not disclosed publicly*	Water or wastewater	Formate/formic acid	Successfully demonstrated CO_2RR for greater than 2500 hours	16
Skyre or sustainable innovations (East Hartford, USA)	Pilot plant	*Not disclosed publicly*	*Not disclosed publicly*	*Not disclosed publicly*	Hydrocarbon fuels	—	46
Siemens and Evonik (Germany)	Lab-scale	CO_2R electrolyzer	Anode: IrO_2 coated titanium, cathode: silver gas diffusion electrode based on oxygen depolarization cathode (ODC used in industrial chlorine–alkaline electrolysis)[47]	0.1 M K_2SO_4/1.5 M $KHCO_3$ as both anolyte and catholyte[47]	~70% selectivity for CO, then CO fermentation to higher alcohols[47]	Stable CO selectivity for almost 1200 hours	15

[a] The information presented in above table is mostly collected from relevant papers or websites. Some companies have not publicly disclosed any data on CO_2 electrolysis amid high competition.

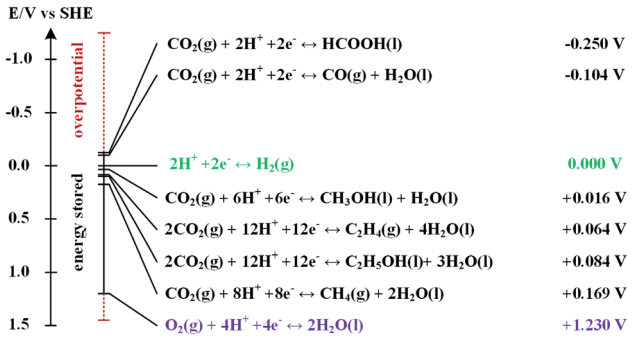

Fig. 2 Standard equilibrium potentials for hydrogen evolution half-cell reaction and several other half-cell reactions to reduce CO_2 into various products at 1 atm and 25 °C. Data presented was taken from Qiao *et al.*[27] (2014).

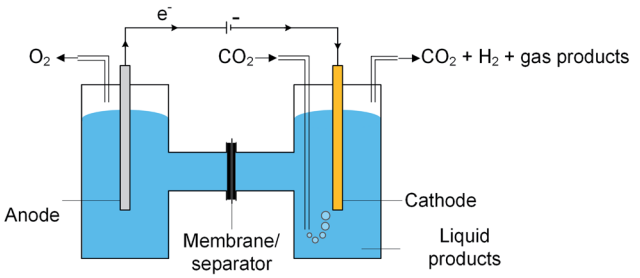

Fig. 3 Schematic of a laboratory electrochemical H-cell (reactor) for CO_2 reduction at the cathode to gas products such as CO and liquid products such as formic acid and methanol with water being oxidized at the anode.

CO_2R, we will look next at the steps involved in transferring CO_2 from the gas phase to the electrode surface.

In most CO_2R electrolyzers, gaseous CO_2 is first dissolved in the liquid electrolyte, then transferred through the liquid to the cathode–electrolyte interface. This process is driven by CO_2 concentration gradients as illustrated in Fig. 4a, and the rate of CO_2 transfer depends on the interfacial contact area, film and overall mass transfer coefficients, and the overall concentration driving force. The concentration gradients in the system are dependent on the solubility of CO_2 in the electrolyte and the selected operating pressures and temperature of the electrolyzer cell. However, prediction of these gradients is complex during CO_2R because acid/base reactions (for example CO_2 consumption by OH^-) in the electrolyte can lead to non-linear deviation of the concentration away from Fick's law behavior,[55] which reduces the concentrations of CO_2 available to react at the electrode's surface.[56] This effect can be partially controlled with buffering electrolytes such as potassium carbonate ($KHCO_3$) to maintain pH at the cathode.[55] The interfacial contact area can maximized by reducing the size of gas bubbles injected to the electrolyte[57] or using a 3D-structured electrode such as a gas diffusion electrode (GDE).[58,59] The magnitudes of CO_2 and CO_2R product mass transfer coefficients generally increase with temperature, pressure, and the velocities of gas and liquid in the electrolyzer, but also are effected by electrolyte density, viscosity and solubility relationships.

Next we examine the cathode–electrolyte interface where CO_2R occurs in a typical aqueous electrolyzer. Cations in the electrolyte migrate towards the negatively charged cathode surface to form an electrochemical double layer (DL), as shown in Fig. 4b. This DL is formed by the outer Helmholtz layer (OHL) of fully-solvated cations, and the inner Helmholtz layer (IHL) of less-solvated halide ions or CO_2-related adsorbed species directly adsorbed at the electrode surface.[49] The presence of this DL can effect CO_2R through several mechanisms. For example, the local electrical field between the negatively charged cathode and the positively-charged adsorbed cations has been reported to stabilize CO_2R-related intermediates such as $*CO_2$ and *COOH.[60,61] On the other hand, in the OHL solvated cations like Li^+, Na^+, and K^+ act as a source of protons for the HER and disrupt the local pH within the DL.[62,63] Another effect relates to interactions between anions and the electrode surface, which have been reported in some cases like I^- and a Cu surface to be strong enough to allow anion absorption within the IHL.[64] In most cases, anions with a pK_a close to the local pH may help buffer the pH and adsorbed ions may be directly involved in CO_2R pathways by affecting the binding strength or adsorption geometry of CO_2R intermediates such as *COOH.[65,66] Fig. 4c illustrates that the concentrations and rates of consumption of protons, CO_2, and other species in the DL are directly proportional to the current density and product selectivity during a CO_2R reaction and these changes in the local reaction environment could occur even at low currents, and thus limit the

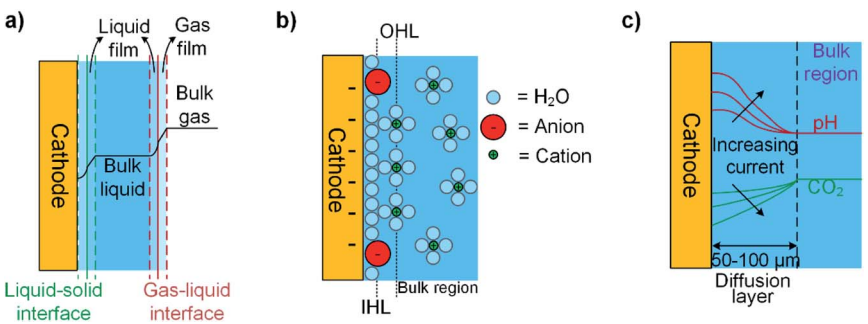

Fig. 4 Schematic illustrations of (a) the concentration profile of CO_2 across gas, liquid, and solid interfaces; (b) the electrochemical double layer with specifically adsorbed anions at the inner Helmholtz layer and solvated cations at outer Helmholtz layer; and (c) changes in CO_2 and pH next to the diffusion layer at increasing current density in a system where CO_2 is supplied from the bulk electrolyte.

overall reaction rate before all available CO_2 becomes depleted at the electrode surface.[53,67]

This background discussion of the principles of CO_2R highlights that even though the electrocatalyst determines the underlying reaction kinetics, other factors such as reactor configuration, electrode structure, and conditions including the type of electrolyte, pH, pressure, and temperature can affect the overall rate of CO_2R reactions.

2.1 Figures of merit to describe electrochemical CO_2R

We briefly describe here the figures of merit commonly used to evaluate and compare electrochemical CO_2R processes. These are faradaic efficiency, current density, and energy efficiency.

• Faradaic efficiency (FE) is the ratio of the amount of charge used to form a product species (*e.g.* CO) calculated from Faraday's law to the total charge (Q) supplied:[68]

$$\mathrm{FE}_{\mathrm{product}} = \frac{ynF}{Q} \quad (2)$$

where y is the number of moles of the product species formed, n is the moles of electrons transferred in the half-cell reaction per mole of product, and F is Faraday's constant.

• Current density (j or CD) is the total current (I, in Amps) per unit area of the cathode (A, m^2 or commonly cm^2) calculated by eqn (3), and describes the total rate of reaction so is an important input to estimate electrolyzer size and capital cost for a CO_2R process.[69]

$$j = \frac{I}{A} \quad (3)$$

Partial current density (j_{product}) for a specific product can be obtained by:

$$j_{\mathrm{product}} = \mathrm{FE}_{\mathrm{product}} \times j \quad (4)$$

• Energy efficiency (EE) is a measure of net energy consumption toward a specific product expressed in eqn (5) as a ratio of amount of energy used to produce the specific product to the net electrical energy supplied to the system.

$$\mathrm{EE}_{\mathrm{product}} = \frac{E^{\mathrm{o}} \times \mathrm{FE}_{\mathrm{product}}}{E^{\mathrm{o}} + \eta} \quad (5)$$

where E^{o} is the equilibrium cell potential for the desired product ($E^{\mathrm{o}}_{\mathrm{cathode}} - E^{\mathrm{o}}_{\mathrm{anode}}$), and η is the sum of overpotentials on the cathode and anode.

3 Electrolyzer configurations

The background discussion in Section 2 highlights how, in addition to catalyst materials, the configuration of the electrolyzer impacts the overall efficiency of a CO_2R process by effecting the limiting rates of CO_2 mass transfer to the catalyst, controlling resistances of cell components, and determining the reaction distribution across electrodes. The two general categories of electrochemical reactors are (i) batch or semi-batch cell and (ii) continuous flow-cell configurations. Batch and semi-batch electrolyzers like the H-cell in Fig. 3a are commonly used in laboratory CO_2R studies with electrodes simply immersed in liquid electrolytes with CO_2 gas bubbled to saturate the catholyte.[70] This configuration is simple, low cost, and allows rapid screening of novel electrocatalysts and electrolytes, but is not practical for treatment of large volumes of CO_2 gases[40,71] because rates of CO_2 mass transfer to the electrode surface (even if the catholyte is vigorously stirred) are too slow and limit CDs to less than 100 mA cm^{-2}.[39] In addition, in a semi-batch cell any cations (*e.g.* K^+) that pass through the separator accumulate in the catholyte, and this accumulation can degrade the electrode kinetics and CO_2R selectivity over extended cell operation or result in high ohmic losses due to electrodialysis.[72,73]

Industrial-scale CO_2R processes require continuous processes to achieve sufficient reaction rates and be economically viable. Table 1 presented examples of continuous flow-cell electrolyzers reported for pilot-plant and scale-up studies, and most of these follow scale-up and engineering strategies that were developed for polymer electrolyte (PE) electrolyzers. In this section we will discuss the separator, which is a critical component in all batch cells and continuous flow-cells, and then describe the liquid-fed, vapor-fed, and microfluidic electrolyzers illustrated in Fig. 5. Our review does not cover flow-field patterns (*e.g.* straight, parallel, serpentine) that can be manufactured on current collectors to optimize CO_2 and electrolyte contact with the catalyst, and to minimize pressure drop, and to manage heat transfer in the cell.[74] We refer readers interested on flow-field patterns to reviews of PE electrolyzers.[74–76]

3.1 Separator considerations

In a CO_2R electrolyzer the separator between cathode and anode chambers, just like separators in water splitting electrolyzers,[73,77] is critical to safe and efficient operation of the cell. An effective separator (1) minimizes the risk of a short circuit between electrodes; (2) prevents exchange of reactants and CO_2R products between cell chambers to reduce the risk of forming unsafe gas mixtures (*e.g.* H_2 and O_2) and prevent oxidation of products at the anode; (3) maintains desired local conditions in the anode and cathode reactions, (4) provides mechanical support to withstand any pressure differences between chambers, and (5) must have a good conductivity for certain ions. The two classes of materials that can provide the required selective ion transport and low permeability to other species are porous separators and ion exchange membranes (IEM). Porous separators include plastic mesh (*e.g.* polyolefin or Netlon) with large pores (0.5–12 mm widths) and microporous diaphragms with pore sizes 0.1–50 μm (*e.g.* glass fibres, polytetrafluoroethylene (PTFE)).[77]

Semi-permeable ion exchange membranes selectively transport certain dissolved ions but are not permeable to other ions or non-charged species. Most CO_2R electrolyzers use monopolar IEMs that are either cation exchange membranes (CEM) such as Nafion® or anion exchange membranes (AEM) such as Sustainion®. Bipolar membranes (BPM) with electrocatalyst

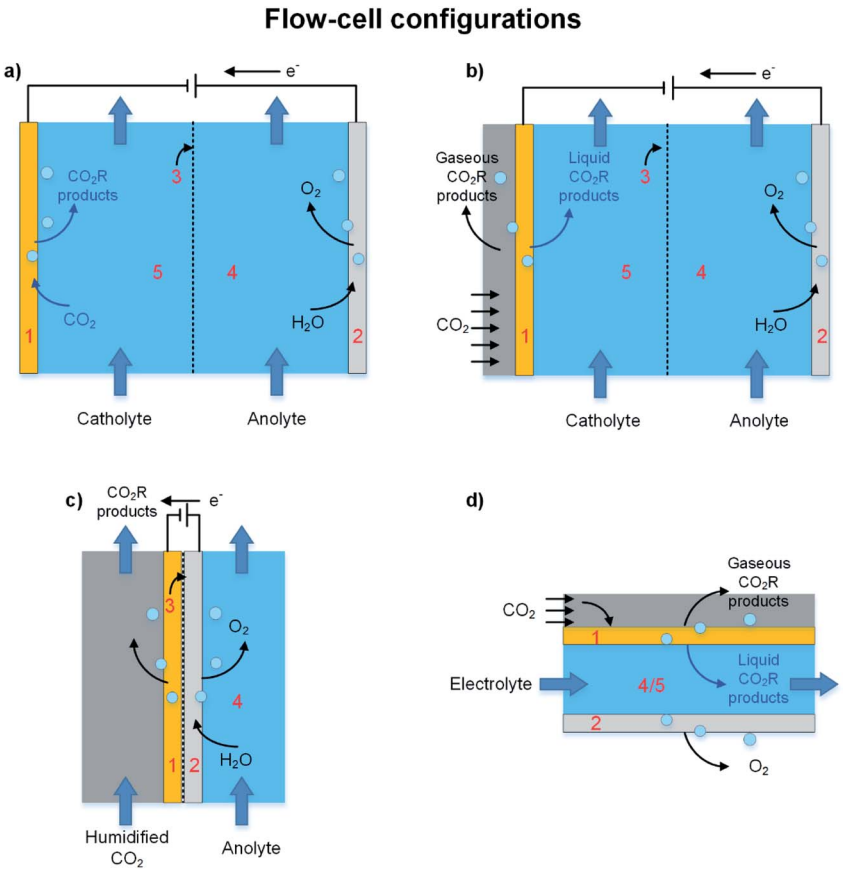

Fig. 5 Schematic of CO_2 electrolyzer in flow-cell configurations (a and b) liquid-fed electrolyzer, (c) vapor-fed electrolyzer and (d) microfluidic reactor. The main cell components are labelled as (1) cathode, (2) anode, (3) separator or ion-exchange membrane which could be a cation exchange membrane, anion exchange membrane, or a bipolar membrane, (4) anolyte, and (5) catholyte.

sandwiched between CEM and AEM layers are also available,[78] and are reported to achieve more stable pH levels between two electrodes at steady state.[79–81] A further advantage of the BPM is that this design may allow lower, cost abundant metals to be used as catalysts instead of precious and noble metals.[82,83] Further detailed descriptions of IEM working principles and recent advances in IEMs are provided in reviews by Kusoglu and Weber,[84] Kaczur *et al.*,[85] Luo and Wessling,[86] and Kimberly *et al.*[87]

The selection of a cation exchange, anion exchange, or bipolar membrane must be considered together with catalyst selection, electrolyte selection, and the targeted CO_2R products. For example, a CEM is commonly used for CO_2R to formate because this IEM blocks formate anions from crossing over to the anode chamber. If the CEM is also proton exchange membrane like Nafion then an acidic anolyte must also be selected to manage proton concentrations,[88] and these decisions limit the choice of OER anode catalysts to expensive precious noble metals such as Ru and Ir. Another consideration for proton exchange membranes is that excess protons will promote HER at the cathode.[89]

Anion exchange membranes can transport anions such as HCO_3^-, OH^- and CO_3^{2-} ions from alkaline catholytes to the anode chamber.[90] Hori *et al.*[91] reported a FE_{CO} up to 92% at 20 mA cm^{-2} which shows the improved performance of AEM-based reactor over CEM. However, there are some important considerations in the use of AEM. For example, CO_3^{2-} and HCO_3^- transported to the anode chamber are expected to produce CO_2, and this reduces the overall efficiency of the CO_2R process. Further, the extended exposure of AEM to alkaline catholytes can lead to blockage of the membrane with less mobile HCO_3^- and CO_3^{2-} anions, which degrades the AEM's ionic conductivity and increases the membrane's ohmic resistance.[87,92–94] In addition, AEM may be susceptible to degradation by excessive OH^-, especially if the membrane is insufficiently hydrated. A recent report by Sun *et al.* revealed CO_2R to methanol and ethanol can also accelerate such degradation.[95]

3.2 Continuous liquid-fed electrolyzers

Fig. 5a depicts a two-chamber liquid-fed electrolyzer in which a CO_2-saturated catholyte and an anolyte are pumped through the separate cell chambers. In this configuration, the catholyte is saturated with CO_2 outside the electrolyzer which requires additional CO_2 capture process units. A more recent integrated design for a liquid-fed electrolyzer is the three chamber cell shown in Fig. 5b that uses a gas diffusion electrode to enhance transfer of CO_2 from the gas phase to the electrolyte–cathode interface. We provide further discussion of GDEs in Section 4.

Obviously, one control on the overall mass transfer rates and thus reaction rate in liquid-fed electrolyzers is the flow-rate of the catholyte because it directly effects superficial liquid velocities in the cell.[96–98] For example, Alvarez-Guerra *et al.*[97] reported that at low current density (CD = 2.5 mA cm^{-2}) the overall rate of CO_2R to formate over a lead-based cathode was insensitive to catholyte flow rates. However, they reported that at higher current densities (12.25–22 mA cm^{-2}) increasing the catholyte flow-rate from 0.57 mL min^{-1} cm^{-2} to 1.44 mL min^{-1} cm^{-2} enhanced formate production because of an improved supply of dissolved CO_2 at the electrode interface for CO_2R.

Both liquid-fed configurations provide larger active electrode area to electrolyte volume ratios than semi-batch cells, and thus can achieve higher overall reaction rates and lower ohmic losses than batch operation.[99–102] An additional advantage of the high electrode area to electrolyte volume ratio in liquid-fed electrolyzers in laboratory studies is that this allows detection of low concentration products and accurate voltage measurement. For example, Kuhl *et al.*[99] used a liquid-fed flow-cell electrolyzer like that in Fig. 5a to detect for the first time acetone, glycolaldehyde, ethylene glycol, glyoxal, and hydroxyacetone as CO_2R products at low concentrations. The expected H_2, CH_4, CO, HCOOH, and C_2H_4 were also reported by Kuhl *et al.* Other groups report also sandwich type compression flow-cells for detection of low concentration products in CO_2R reactions.[57,63,101,103,104]

Fig. 6a shows an example of a liquid-fed electrolyzer with a BPM separator that due to the better control of pH imparted by the BPM achieved a more stable cell voltage during a 12 hour CO_2R experiment than an electrolyzer with a CEM (Fig. 6b and c).[71] However, a potential issue with BPMs in liquid-fed electrolyzers is ensuring the rate of water flux across the BPM matches the rate of water dissociation to prevent dry-out of the membrane, which leads to significant increases in ohmic resistance.[105] Another potential issue in liquid-fed electrolyzers is that the ionic conductivity of the BPM depends on the concentration-gradients of salts in the electrolyte,[106] and because a BPM inherently leads to depletion of charge at the CEM/AEM interface this can create significant junction gradients. Therefore, operation of liquid-fed electrolyzers with BPMs requires ion concentrations in both the catholyte and anolyte to be controlled for the reaction kinetics and for the material and thickness of the membrane(s).

In liquid-fed electrolyzers with a GDE, unstable CO_2R operation can result from liquid flooding of the GDE. Several researcher groups suggest suppling the CO_2 gas at higher pressures to prevent liquid ingress into the GDE and in this case any gaseous CO_2R products leave the electrolyzer with the catholyte.[54,107–109] For example, Haas *et al.*[47] operated a liquid-fed electrolyzer at 50 mA cm^2 for more than 1000 h, but report that to achieve this current density they had to sacrifice CO selectivity. Jeanty *et al.*[110] ran a CO_2 electrolyzer at 150 mA cm^2 with a CO FE close to 60% for more than 200 h over a 100 cm^2 electrode area. A potential adverse effect of operating with a high gas overpressure across the GDE in a liquid-fed electrolyzer is that the higher partial pressure of CO_2 leads to precipitation from the bicarbonate/carbonates catholyte which can reduce electrolyte conductivity, block GDE pores or modulate pH. All such effect increase the overall ohmic losses in the cell.

3.3 Vapor-fed electrolyzers

Fig. 5c shows a vapor-fed flow-cell electrolyzer[111] with an IEM coated on one-side with a cathode catalyst and on the other side with an anode catalyst to create a zero-gap cell. In this configuration, the catholyte is supplied *via* humidified CO_2-containing gas to maintain membrane hydration during CO_2R. Compared to liquid-fed electrolyzers, the key advantages of vapor-fed electrolyzers are lower ohmic losses and reduced risk of catalyst poisoning from impurities in the catholyte. In addition because the vapor-fed cell does not require pumps to feed the electrolyzer the equipment and operating costs may be lower than a liquid-fed cell; however, this comparison depends on the cost of the processes required to vaporize catholyte into

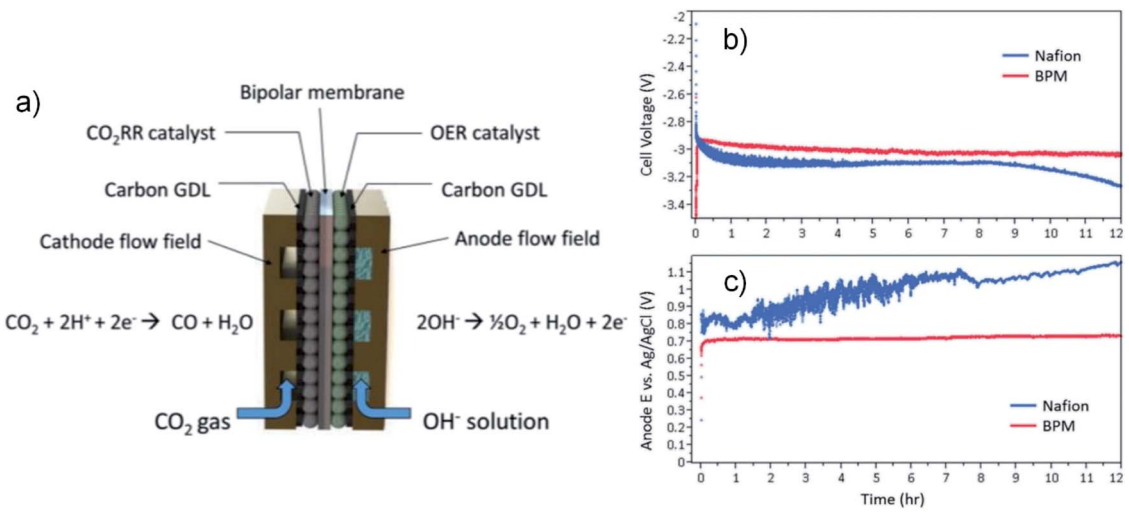

Fig. 6 (a) Schematic diagram of a CO_2 electrolyzer employing a BPM; comparison of (b) overall cell voltage and (c) anode potential *vs.* Ag|AgCl between BPM and Nafion membrane. 0.1 M KOH was used as anolyte and 0.5 M $KHCO_3$ as catholyte. Reprinted with permission from Li *et al.*,[71] Copyright 2016, American Chemical Society.

the CO_2 feed gas. One potential drawback of vapor-fed electrolyzers is liquid CO_2R products like alcohols can flood back into GDE pores and thereby hinder CO_2 access to the active sites.

Most vapor-fed electrolyzers reported in the literature use a CEM to transport protons from the anode chamber to the cathode for CO_2R. For example, Lee *et al.*[112] reported more stable formate production over a tin nanoparticle cathode catalyst in a vapor-fed electrolyzer than a liquid-fed electrolyzer, and they attributed the improved performance to a shorter CO_2 diffusion pathway to the catalyst. However extended CO_2R operation in CEM vapor-fed electrolyzers is reported to lead to acidification at the cathode, which promotes unwanted HER.[113] In an alternative design, Kutz *et al.* used AEM like a methylimidazolium-based styrene polymer in a vapor-fed electrolyzers with Ag-based catalyst and reported stable operation for 6 months at CD = 50 mA cm^{-2} with a FE_{CO} = 90%.[43] Mallouk's laboratory[71] reported a vapor-fed electrolyzer with a BPM separator and ionic liquid catholyte that achieved CDs two times larger than a liquid-fed cell and relatively stable cell voltage close to 3 V during operation at 80 mA cm^{-2} for 14 h. However, they did report that the FE_{CO} began to degrade after 1 h, which may have been due to de-wetting of the ionic liquid IL from the surface of the catalyst.[71] Salvatore *et al.*[114] enhanced the stability of this vapor-fed with BPM configuration using a solid support layer of aqueous $NaHCO_3$ between the Ag-decorated GDE and the BPM, and demonstrated a steady FE_{CO} = 65% at 100 mA cm^{-2} and 3.4 V for 24 h.[114]

3.4 Microfluidic electrolyzer

A microfluidic electrolyzer (Fig. 5d), such as the cells described by Kenis and co-workers,[115,116] does not use a membrane separator but instead uses a thin (less than 1 mm) electrolyte flow-field channel to separate electrodes. In this configuration gaseous CO_2 diffuses to the electrode–electrolyte interface through a gas diffusion layer (GDL), and crossover of reactants and products is controlled at laminar flow conditions because diffusion of the products is slow. Due to its compact design and high surface area to volume ratio, a microfluidic electrolyzer design could allow fast rates of CO_2 mass transfer to the cathode surface and thus high CDs for CO_2R.[115,116] Additionally, microfluidic electrolyzers may provide new opportunities for fundamental studies into the effects of temperature, pH, catalyst deposition methods, electrolyte composition, GDL composition, and channel length on CO_2R processes and thus help provide new insights for technology improvement.[115,117]

3.5 Separation of CO_2R products downstream of the electrolyzer

Efforts towards improving the selectivity of CO_2R through catalyst innovations and optimization the electrolysis process are aimed partly at increasing the concentration of products in the electrolyzer effluents so as to the cost of product separation processes.[118,119] Greenblatt *et al.*[120] showed just how energy intensive separation of liquid products from a photoelectrochemical CO_2R could be, with 4.7 to 45 MJ kg^{-1} of product required using distillation to recovery products from 10 wt% to 1 wt% in the catholyte stream from the electrolyzer.[120] Greenblatt *et al.* reported more energy efficient technologies such as membranes and solvent extraction could potentially reduce the energy requirements to 0.1–8.3 MJ kg^{-1} product, but these technologies cannot always compete with distillation in terms of higher throughput and desired purity.[120]

One strategy to avoid separation costs could be direct use of effluent streams from the CO_2R reactor. For example, potential opportunities could include tuning the CO_2R performance tuned to produce CO + H_2 mixtures to feed a Fischer–Tropsch process, CH_4 + C_2H_4 mixtures for synthesis of C_3H_6,[121] or alcohol and/or hydrocarbon mixtures for liquid fuels.[122,123] However, that strategy is likely only viable in a small number of circumstances where the CO_2 source and the potential use of CO_2R products are closely located and integrated. Therefore, consideration must be made for separation of CO_2R product streams. One of the challenges with CO_2R processes compared to many other industrial conversion processes is that the concentration of products, especially liquid products, leaving the electrolyzer are low. For example, in the conventional formic acid route of hydrolysis of methyl formate produces formic acid + methanol mixtures with more than 10% formic acid that are relatively easy to separate by distillation or liquid/liquid extraction.[124,125] However, the concentration of formic acid leaving a CO_2R electrolyzer is typically less than 1% in a mixture of water and the electrolyte salts. Recovery of the formic acid from this CO_2R effluent stream requires an acidification process then azeotropic separation to obtain a pure formic acid product. Furthermore, formic acid separation processes are sensitive to pH like acidification and potential inorganic salts separation (*e.g.* crystallization) so conditions in the electrolyzer may affect downstream process.[126]

Control of the engineering factors described in the article (*e.g.* reactor design, electrode structure, electrolyte, pH, pressure, and temperature) may ultimately help to design efficient downstream separation processes. For example, the choices of conducting salts, solvents, IEMs, and flow rates can all effect the concentration and types of liquid CO_2R products that must be recovered from the electrolyte. Yang *et al.*[127] provide a clear demonstration of the relationships between reactor design and product distribution in their report of electrolyzer with a Sustainion™ AEM to obtain streams with up to 20 wt% formic acid from the reactor. In summary, the overall reactor design is a key factor that governs the properties of the CO_2R product streams.

4 Electrode structure

The cathode in a CO_2R electrolyzer must provide active catalyst sites, facilitate sufficient contact between CO_2, electrolyte and catalysts, and conduct electrons. Fig. 7 depicts the three types of cathode architectures: (a) planar electrodes (*e.g.* a metal foil or glassy carbon plate),[128–133] (b) simple porous electrodes (*e.g.* carbon paper or mesh),[134–138] and (c, d) gas-diffusion electrodes (GDEs).[139–141] Most CO_2R electrocatalyst screening and fundamental catalysis studies[30,31,47,142–144] use planar electrodes or simple porous electrodes because these types are relatively simple to construct and immerse in a CO_2 saturated electrolyte

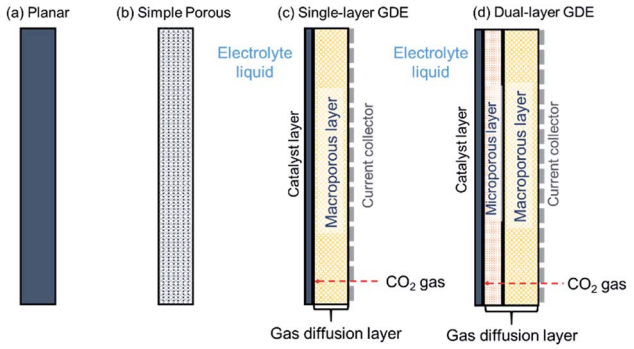

Fig. 7 Schematic diagrams of (a) planar electrode, (b) simple porous electrode, (c) single-layer gas diffusion electrode (GDE), and (d) dual-layer GDE.

(for example, in a electrochemical cell like that shown in Fig. 3a).

The planar electrode is useful to screen catalyst materials in a laboratory scale because of its relatively simple geometry that rules out impacts induced by complex factors such as structures of the electrodes. In addition, placement of a reference electrode is straightforward, thereby enabling single electrode overpotential measurements. However, the CO_2R half-cell reaction rates achieved with a planar electrode or porous electrode are often limited by the rate of CO_2 transfer across the hydrodynamic layer from the bulk electrolyte to the electrode surface especially at a high CD.[58] In such systems, mass-transfer rates could be improved by operating the electrolyzer at high pressure, low temperature, or selecting organic electrolytes to increase the solubility of CO_2 in the electrolyte. But those options add costs and complexity to the CO_2R process.

For high CD electrolyzers, one prefers the application of the last three electrode types (Fig. 7b–d) that are 3D-structured catalytically-active materials or electron conducting material with coverage of catalysts. A 3D-structure increases the active electrode area and decreases the transport resistance of gaseous and liquid reactants and products. Increasing the active electrode area reduces overall cell voltage and increase the rate of charge and mass-transport. Fast charge and reactant transport also accelerate the electrode kinetics. However, challenge arises in understanding the property-performance relationship and optimisation of the 3D-structure for efficient CO_2R conversion. This results from the complexity of the 3D-structured electrodes that involves multiphase flow in the pores, interactions at interfaces and multiscale kinetics at the catalysts. Though this area still remains underexplored in CO_2R application, a lot can be drawn from the studies in other electrochemical conversion applications such as PEM fuel cells and redox flow batteries. Recently, Shojaeefard *et al.*,[145] Weber *et al.*,[146] and Fadzillah *et al.*[147] reviewed the electrode microstructure restructuring and pore-scale simulations. Moreover, Lai *et al.*[148] and Walsh *et al.*[149] reviewed the design and fabrication of general 3D-structured electrodes, including the 3D-electrode architecture and decoration of catalysts.

Overall, the ultimate goal of developing 3D-structured electrode is to minimise the various cell resistances due to electron and ion transport, multiphase flow (*e.g.* bubble), transport-related, and electrochemical reaction. The ohmic resistance of 3D-structured electrode is mainly influenced by both the 3D-skeleton and the interfacial conductivity. The 3D-electrode structure is a composite made of conductive matrix (carbon or metals) and less-conductive binders (*e.g.* PTFE or ionomers) and/or pores containing electrolyte or gas, thus requiring multiple percolations pathways for reactant molecules, ions and electrons.[150–152] Simply put, increasing porosity decreases the overall conductivity of the matrix and therefore increases the overall ohmic resistance. The interfacial conductivity, governed by the interfacial contacts and heterogeneous phases, contributes more to the ohmic resistance. This is valid especially for a pure metal matrix as prepared through sintering, where sintering temperature, interfacial contact and sizes of metal particles and pore formers are important factors to consider.[151] 3D-structured electrodes decorated with heterogeneous catalyst materials also have extensive interfaces between the conductive backbone and less conductive catalysts, thus facing an increase of ohmic resistance. Therefore, the size and shapes of the catalysts and pore structures of the matrix also matter for the overall electrical conductivity of the structure.[153] Compared with the ohmic resistance, the resistance related to transport is more critical, particularly for mass-transport-controlled CO_2R electrolysis.[111] In a 3D-porous electrode, transport of liquid and/or gas reactants and products is dominated by either molecular or Knudsen diffusion, depending on the pore size and electrode structures. Similarly, wettability and pore size dominate the intrinsic saturation/capillary-pressure relationship that is critical for optimal multiphase performance.[146]

The electrochemical reaction resistance is related to the electrode kinetics. In addition to the catalyst materials (where compositions, surface orientations, morphology, and sizes are important factors) that directly affect the kinetics, catalyst support, multiphase flows within the electrode and local environments are all crucial for CO_2R surface reaction rate and selectivity. For the effects of catalyst support, one could refer to a recent review published by Li, MacFarlane, and Zhang,[30] as well as herein. However, there are still gaps remaining, especially regarding the exact interfacial structure of the catalysts (especially with ionomer),[146] and how these structures affect the electrode kinetics. Answering these questions is essential to guide where and how to deposit catalysts in the electrode structure. It is also important to note that an optimal balance has to be achieved among these resistances. For example, oxide-derived catalysts are active for CO_2R[154,155] but may not be very electrically conductive, leading to a decrease of electrode kinetic resistance but an increase of ohmic resistance. In the case where liquid products are targeted products, a high reaction rate consumes quickly the CO_2 gas and lowers the local gas pressure, which may lead to local flooding that blocks gas transport and in turn degrades CO_2R selectivity. Such a balance appears more crucial in the GDEs that include the transport of gases in the electrode structure. Because recent works have

demonstrated a superior CO_2R performance of GDEs compared to planar and simple porous electrodes, in the following subsections we mainly focus the review of recent GDE development for CO_2R.

4.1 Gas diffusion electrodes

GDEs offer an alternative approach to improve mass-transfer and overall CO_2R rates.[156,157] The key difference between a GDE and a simple porous electrode is that in a GDE, the CO_2 gas diffuses through a gas-diffusion layer (GDL) to the electrode–electrolyte interface inside the catalyst layer (CL). This type of GDE electrolysis has been reported to achieve reaction rates up to an order of magnitude faster than porous electrodes that require CO_2 transfer from the bulk electrolyte to the electrode surface.[58] A typical GDE, as shown in Fig. 8, consists of a GDL, a CL, and a current collector as shown in the two examples in Fig. 7c and d. The porous metal mesh or foam current collector serves to distribute current and maybe engineered with gas flow channels.[142,158–160] The porous GDL should enable fast transport of gaseous CO_2 to the CL, where the electrochemical reactions occur. A critical property of the GDL is that this layer must be hydrophobic (or more generally, the GDL must be gas wet relative to the wetting with electrolyte) to prevent liquid electrolyte from seeping to the gas flow channel. The GDL can be designed with a single-layer of porous materials (Fig. 7c) or dual-layers with different porosities and wettabilities (Fig. 7d). In a single-layer GDL, the hydrophobic macroporous layer might be a metal mesh or metal foam, or a hydrophobically-treated porous carbon such as polytetrafluoroethylene (PTFE) treated carbon paper. A dual layer GDL (Fig. 7d) includes a macroporous layer and a microporous layer (MPL).[161] The MPL is normally a hydrophobic layer with small pores that is composed of carbon powder and PTFE.[162] The catalyst layer (CL) is commonly prepared by depositing the catalytically active phase, including catalysts and an ionic binder on the GDL or membrane.

In a recent publication, Weng, Bell and Weber predicted with a mathematical model that a Ag-based GDE could potentially achieve a partial CD (PCD) for CO one order of magnitude higher than that achieved with a planar Ag electrode.[58] That study concluded that good GDE performance is achieved by (1) a high density of active sites per geometric electrode area, and (2) a low mass-transfer resistance in the GDE, especially at more negative potentials. The predictions of the Weng, Bell and Weber modelling study are consistent with various experimental studies.[58] For example, Castillo *et al.* reported that a Sn-based GDE with 1.5 mg Sn cm^{-2} achieved a maximum FE of ~70% in producing formate at a current density of 40 mA cm^{-2}, which was more efficient than the planar Sn electrode with a maximum formate FE of 67% at 12 mA cm^{-2}.[163] In another example, Hass *et al.*[47] demonstrated a commercial Ag-based GDE, which was developed by Covestro as an oxygen depolarized electrode (ODE) for chlor-alkali applications, as a cathode in a CO_2 flow cell electrolyzer with stable operation at a CD of 300 mA cm^{-2} and CO FE close to 70% for over 1200 h. A brief summary of other recent reports of GDEs as cathode for CO_2R is provided in Table 2.

Although only a relative small number of studies report use of GDEs for CO_2R,[141,157,159,171] GDEs have been extensively developed and optimized for fuel-cell applications.[161,172,173] The knowledge from this field can be leveraged to develop more efficient GDEs for CO_2R, but the requirements for CO_2-electrolyte contacts in a CO_2R electrolyzer are more challenging than in a fuel cell. We describe in the following sections recent advances to optimize GDEs for use as the cathode in a CO_2R electrolyzer.

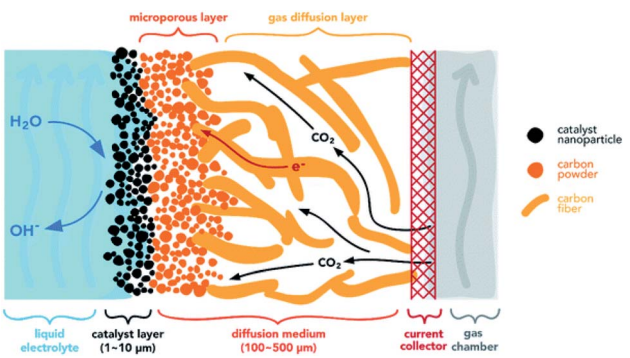

Fig. 8 Schematic diagrams of a gas diffusion electrode.[58]

4.2 Engineering the gas diffusion layer

4.2.1 Macroporous layer. As one of the key components of GDE, the GDL normally (1) serves as a mechanical support for the CL, (2) allows an easy diffusion of the gaseous CO_2 and release of gas products such as CO and CH_4 through its pores at the reaction sites, (3) enables electron conduction from the current collector to the CL, and (4) prevents the electrolyte from seeping to the gas channel. The macroporous layer of the GDE can be fabricated by (1) mixing the carbon materials (*e.g.* acetylene black[142,164,174,175] and carbon fiber) with PTFE[164] or Teflon,[174] (2) hydraulic pressing or rolling[176] the mixture with or without current collector to form the film, and (3) sintering the film at 340 to 380 °C. The sintering temperature is slightly above the melting temperature of the hydrophobic agents, so that the agents can bind strongly with the carbon materials. In most cases, however, commercially available carbon papers (*e.g.* Toray or SGL carbon papers) have been used as the macroporous layer of the studied GDEs.

The thickness and hydrophobicity of the macroporous layer predetermine the mass-transfer resistance of CO_2 in the GDEs, and thus have an impact on the CO_2R reaction rate. For example, Kim *et al.* compared the CO_2 gas permeability and CO_2R performance over Ag-based GDEs with carbon-fiber substrates (*i.e.* macroporous layer) in different thicknesses ranging from 170 to 380 μm.[162] With the reduction of substrate thickness from 370 to 190 μm, they found that the CO_2 gas permeability increases from 69.25 ± 0.69 to 72.42 ± 0.72 mL min^{-1}, and that the PCD of CO also improves from ~180 to ~220 mA cm^{-2} at −2.05 V *vs.* Ag|AgCl. The enhanced PCD of CO_2R for thinner substrates is attributed to the improved CO_2

Table 2 A summary of recent works on GDEs as cathode for CO_2R

Catalyst material	Catalyst loading	GDE configuration	Current collector	Remarks	Reference
Ag	NA	Dual layer	NA	Oxygen depolarization cathode (from Covestro)	47
Ag	0.8 mg cm^{-2}	Dual layer	Carbon	20 wt% PTFE MPL, 10 wt% carbon fiber substrate 190 μm	162
Cu	20 nm	Dual layer	Carbon	(20 nm thick catalyst layer)	45
Cu (−350 mesh, 5N purity)/carbon	NA	Single layer	Cu gauze	Cu mixed with carbon black (CB, hydrophilic) and $CB_{hydrophobic}$ as the catalyst layer, Cu/($CB_{hydrophilic}$ + $CB_{hydrophobic}$) = 1.2	164
Cu	7 mg cm^{-2}	Single layer	Cu grid		157
Cu_2O/ZnO	1 mg cm^{-2}	Single layer	Carbon	Air brushed on porous carbon paper	165
In/C	1 ± 0.05 mg cm^{-2}	Single layer	Carbon		140
$La_{1.8}Sr_{0.2}CuO_4$	NA	Single layer	Stainless steel mesh	Carbon/Teflon	141
Pt	0.56 mg cm^{-2}	Single layer	Stainless steel mesh		159
Pt/CNTs	NA	Dual layer	Carbon	Sigracet 25 BC GDL with imidazolate-based SIM-1	166
Sn	NA	Single layer	Carbon	Sn electrodeposited on carbon fibers	167
Sn	1.5 mg cm^{-2}	Single layer	Carbon	Sn on Toray carbon paper	163
Sn	1.9 mg cm^{-2}	Dual layer	Carbon	Sn electrodeposited on dual layer GDL	168
Sn	5 mg cm^{-2}	Single layer	Carbon	11.1 wt% PTFE in catalyst layer	169
Sn nanoparticles (10–15 nm)	0.75 mg cm^{-2}	Dual layer	Carbon		144
Sn@Cu	NA	Dual layer	Cu mesh	Sn loaded on a Cu mesh through electroless deposition, and subsequently rolled on the GDL	160
Sn	NA	Single layer	Carbon	Sn electrodeposited on carbon fiber paper	170

gas permeability. However, a too thin substrate (Toray Carbon Paper 30 with a thickness of 110 μm) leads to electrolyte flooding (*i.e.* the electrolyte fully occupies the pores) in the GDE during the CO_2R operation, in essence turning into a simple electrode case. Therefore, an optimal thickness of the microporous layer is essential to ensure a balanced gas permeability and effective electrolyte management in the GDE.

Another key factor is the wettability of the macroporous layer: too high a hydrophobicity may cause poor electronic conduction due to the high amount of non-conductive hydrophobic agents, while too high of a hydrophilicity may limit the diffusion of CO_2 due to flooding propensity and promote unwanted HER.[40,58] The wettability can be adjusted by controlling the content of hydrophobic agents (*e.g.* PTFE),[161,177,178] and hydrophilic treatments (such as plasma treatments, addition of inorganic oxides or carbon black, *etc.*).[161,179,180] Ikeda *et al.* observed similar CO_2R reaction rates for the macroporous layer with PTFE contents between 10 and 30 wt%, but a degraded performance for the one over 30 wt%.[164] A recent detailed investigation on Ag-based GDE showed that the macroporous layer with 10 wt% of PTFE has a higher CO PCD of 224 mA cm^{-2} than those with PTFE content of 30 wt% (PCD = 190 mA cm^{-2}) and 50 wt% (PCD = 158.41 mA cm^{-2}) at −2.05 V *vs.* Ag|AgCl.[162] (Fig. 9a) The better performance for the GDEs with lower PTFE content in macroporous layer is a consequence of the better electronic conduction than those with higher PTFE content, as evidenced by the observed lower charge-transfer resistance from the electrochemical impedance spectra (Fig. 9b). In the studied PTFE range (10 to 50 wt%), additionally, the authors observed negligible effects of the PTFE content in the macroporous layer on the CO_2 gas permeability and durability of the GDEs.

4.2.2 Microporous layer. As compared with the macroporous layer, the MPL is normally a thinner porous layer with smaller pore sizes and volumes, and is sandwiched in between the macroporous layer and CL. A comparison of scanning electron micrographs of GDE with or without MPL is shown in Fig. 10b and d, respectively. The fabrication procedure of MPLs is similar to the processes to make the macroporous layer. The mixtures of carbon black and hydrophobic agents are casted onto one side of the macroporous layer, followed by sintering treatment to ensure sufficient bonding.[144,162] One should note that the carbon-based materials normally contains metal residues such as Fe, Co and Ni.[181–183] As the MPL is in direct contact with the catalyst layer, these metal impurities in the carbon materials may promote unwanted HER during the cell operation. Therefore, cleaning the MPL or the whole GDL in highly concentrated acid is highly recommended to minimize the content of metal impurities before deposition of catalyst layer. As shown in the Table 2, not all of the GDE-based cathodes for CO_2R contain MPLs. Research in polymer electrolyte fuel cells have demonstrated that the MPL layer not only plays a key part in maintaining separation between liquid and gas, but also

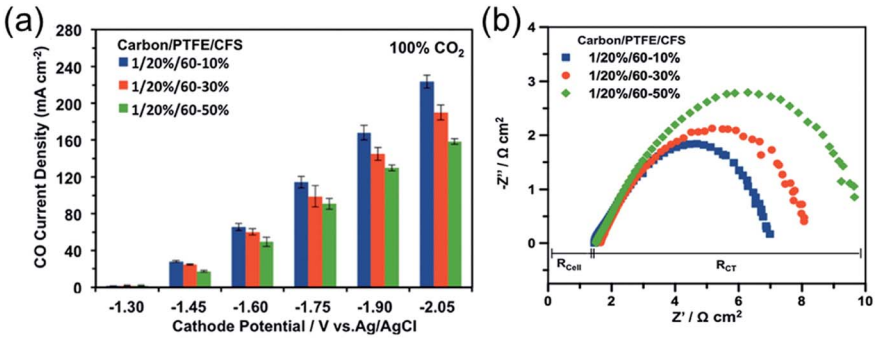

Fig. 9 (a) A comparison of GDE with 10, 30, and 50 wt% PTFE in the macroporous layer as a function of potential. (b) The Nyquist plot of electrochemical impedance spectra of the corresponding GDEs at −2.0 V *vs.* Ag|AgCl. CFS means the carbon fiber substrate, which is the macroporous layer of the GDE. R_{cell} represents the ohmic resistance of the cell, and R_{CT} is the polarization resistance related to charge transfer. Reprinted with permission from Kim *et al.*,[162] Copyright 2016, Elsevier Ltd.

provides the electrode with improved interlayer contact, lower electrode ohmic resistance, higher CL temperatures, and better structural integrity.[161,184] For the application of CO_2R, Kenis *et al.* found that the MPL in the GDE could provide a support for the CL and prevent potential flooding in the macroporous layer.[162] The MPL can also prevent the exposure of the carbon fiber to the electrolyte (Fig. 10a–d) and thereby suppressing the undesired HER catalyzed by the exposed carbon fibers. As a result, the presence of MPL in the GDE-based cathode contributes to a significantly improved CD as high as ~220 mA cm^{-2}, ten-fold higher than the one without MPL at −2.2 V *vs.* Ag|AgCl[162] (Fig. 10e).

Additionally, in the same work, the authors also studied the effects of PTFE content of the MPLs on CO_2R reaction rate. As shown in Fig. 11a, the CO PCD increases with PTFE at low PTFE contents ≤20 wt%, but decreases with PTFE at contents >20 wt%.[162] Too little PTFE content (*i.e.* 4.5–10 wt%) in the MPL is insufficient to prevent flooding of the layer by electrolyte and does not provide strong binding between the carbon and catalysts in the CLs, which resulted in the higher HER level and poorer cathode durability. A higher content of PTFE (>20 wt%) in the MPL degrades the electronic conductivity of the GDE (Fig. 11b) and also reduces the MPL porosity.[185] Correspondingly, both the resistances of GDE for electron transfer and CO_2 mass transfer become higher, thus leading to a degraded CO_2R performance.

4.2.3 CO_2 adsorption layer. A CO_2 adsorption layer can also be incorporated at the GDL surface facing the CO_2 to further promote the CO_2R. For example, by covering a substituted imidazolate-based metal–organic framework (SIM-1) on a macroporous layer, Marepally *et al.* significantly improved the performance over a Pt/carbon nanotube (CNT)-based GDE, with an increased rate of CO_2R products, including methanol, ethanol, acetone, and isopropanol, by 1.5 times as compared with the counterpart without the adsorption layer.[166] Such remarkable >C1 production improvement, as brought by deliberately concentrating the surface CO_2 through the adsorption layer, highlights the essential roles of electrode design, in addition to the effects from electrocatalysts, in controlling the CO_2R pathways.

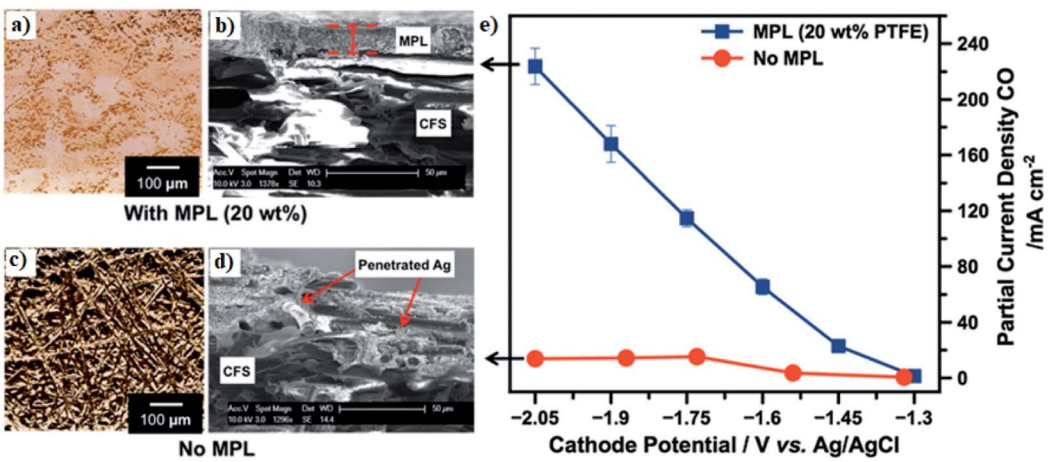

Fig. 10 (a and c) Micro-computed tomography and (b and d) SEM images of Ag-based GDE with and without the microporous layer. (e) A comparison of CO partial CD of Ag-based GDE with and without MPL as a function of potential. Reprinted with permission from Kim *et al.*,[162] Copyright 2016, Elsevier Ltd.

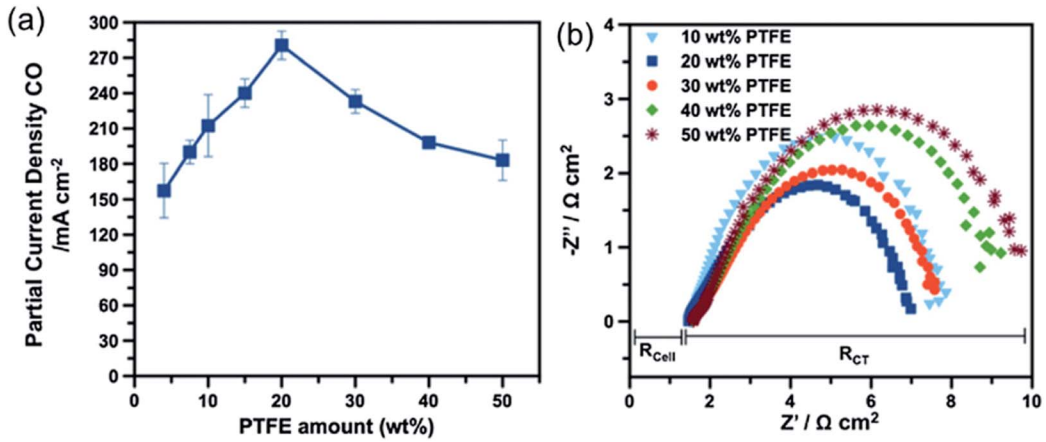

Fig. 11 (a) A comparison of PCD of CO for Ag-based GDE as a function of PTFE content in the MPLs. (b) The Nyquist plot of electrochemical impedance spectra for the corresponding GDEs at cathode potential of −2.2 V *vs.* Ag|AgCl. Reprinted with permission from Kim *et al.*,[162] Copyright 2016, Elsevier Ltd.

4.3 Optimization of the catalyst layer

The CL is mainly a layer of the electroactive cathode materials normally immobilized on one side of the GDL (typically on the MPL) facing the electrolyte or membrane through various deposition methods (*e.g.* electrodeposition,[168] drop casting,[45] thermal evaporation,[45] ionic displacement, or pressing[139]), though the position of the CL can be also extended inside the GDL structure to further increase the electroactive interface boundaries.[186] There are several factors that could contribute to the activity and product distribution of the CO_2 electrolysis, such as the catalyst materials, catalysts loading (*i.e.* the mass of catalyst per electrode geometric area), ionic binders, and CL deposition methodology.

Immense research efforts have been and continue to be devoted to the study and development of catalyst materials suitable for CO_2R, and the recent advances in the catalyst development have been extensively reviewed recently.[28,30,31,187,188] Most of these studies mainly focused on catalysts supported by a planar electrode or simple porous electrode, but not by a GDE, where the CL must deal with complex transport and reaction processes simultaneously and there is an inherent need for porosity.

The processes taking place at the CLs of GDE cathodes are even more complex than those in the GDL, since all of those processes occur as well as the electrochemical reactions and ionic transport. Weng *et al.* recently discussed in detail regarding the processes involved in the CL of an Ag-based GDE.[58,189] In addition to local environment change close to the electrode surface in the electrolyte during CO_2R operation, as discussed in the electrolyte selection and pH effects sections, the CL of the GDE also needs to manage the transport of gas and ions to achieve an optimal cathode performance. Too dry of a CL results in catalytically active sites becoming inactive due to the absence of supporting electrolyte or ionic pathways, but flooded pores increase the mass-transfer resistance of gaseous CO_2. An ideal CL should facilitate a sufficient contact of liquid electrolyte and gas with the catalysts. Furthermore, the reaction kinetics are intimately connected with the transport phenomena. What also matters is the pore size in the CL. Small hydrophilic pores will be flooded when the liquid/gas pressure difference is low. When the pressure difference between gas and electrolyte increases, the susceptibility to electrolyte flooding of the pores in CL follows the trend: large hydrophilic pores > large hydrophobic pores > small hydrophobic pores.[58]

The amount of catalysts loading in the CL also alters the CD and product distributions. For example, through varying the Sn catalysts loading content ranging from 0 to 15 mg cm^{-2}, Kopljar and co-workers found that a higher content of Sn increases the CO_2R activity as evidenced by the observed higher CD and lower Tafel slope, especially at the higher potential range as shown in Fig. 12a.[139] Such enhancement could be a result of the increased concentration of catalytically active sites as imparted by the higher Sn loading. Moreover, the product distribution was also found to be dependent on the catalyst loading: a Sn loading of less than 5 mg cm^{-2} could lead to ~90% of FE for $HCOO^-$ formation, <10% for CO and 3% for H_2, and further increase of the loading decreases the selectivity of the $HCOO^-$ production but promotes CO and H_2 evolution (see Fig. 12b). The authors considered the effects of catalyst loading on product distribution analogous to the effects of cathodic potentials, where a low cathode potential leads to the promotion of CO and H_2. Alternatively, we explain such phenomena by two possible reasons. First, a higher Sn loading may hamper the diffusion of CO_2 to the active regions and therefore lead to the promotion of HER. Second, similar to the effects of interparticle interactions on Cu nano-particles for CO_2R catalysis,[190] a higher catalyst loading could increase the availability of neighboring active sites and therefore promote re-adsorption of $HCOO^-$ for further reduction to become CO as the final product.

Sargent *et al.* recently used Cu-based GDEs with a very thin Cu CL (*i.e.* 10 or 25 nm thick) as the CO_2R cathode to achieve a higher CD and higher FE for C_2H_4 formation than the ones with thicker Cu CLs (*i.e.* 1000 nm thick and ~1000 μg cm^{-2} CL) at a higher cathodic potential (*i.e.* <−0.54 V *vs.* RHE).[45] At lower cathodic potential (>−0.4 V *vs.* RHE), in contrast, the GDEs with

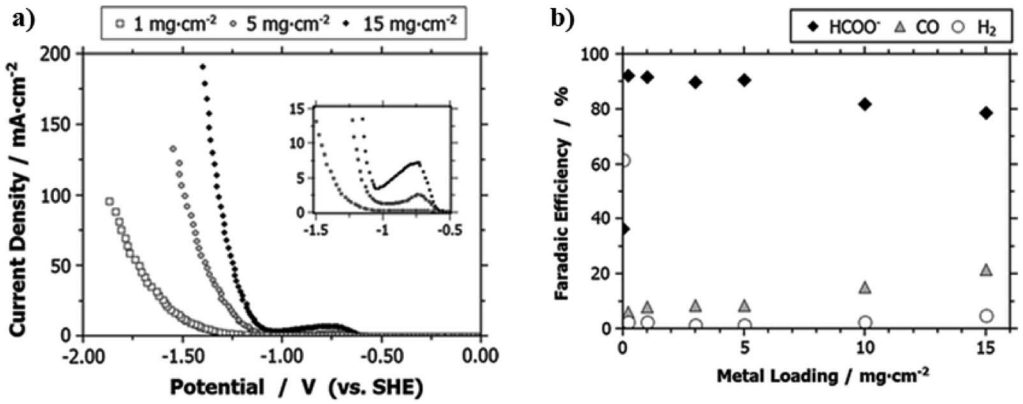

Fig. 12 (a) A comparison of CD for GDEs with various Sn loading as a function of potential. (b) The FE for $HCOO^-$, CO and H_2 production for GDEs with different Sn loading at 50 mA cm^{-2}. All the experiment were conducted in the 0.1 M $KHCO_3$ aqueous electrolyte. Reprinted with permission from Kopljar *et al.*,[139] Copyright 2014, Springer Nature.

thick CLs exhibited higher CDs than the thin CLs. They explained the higher FE for GDE with the thin Cu CLs by the catalyst-mediated abrupt interface as imparted by the thin layer of Cu, which could accelerate the rate-determining CO dimerization step for C_2H_4 formation.[45] It could be thought that the thin layers and high flowrates of electrolyte also did not provide sufficient time for the homogenous acid/base reactions of CO_2 to occur, thus resulting in higher CO_2 local concentrations compared to the thicker CLs, where the CO_2 and electrolyte residence time was higher. The multi-physics model of Ag-GDE developed recently for CO_2R showed that a thinner CL could enhance the mass transfer of the CO_2 in the GDE, which normally dominates the overall reaction rate at high cathodic potential.[58,189] Consequently, the negative effect on CD due to

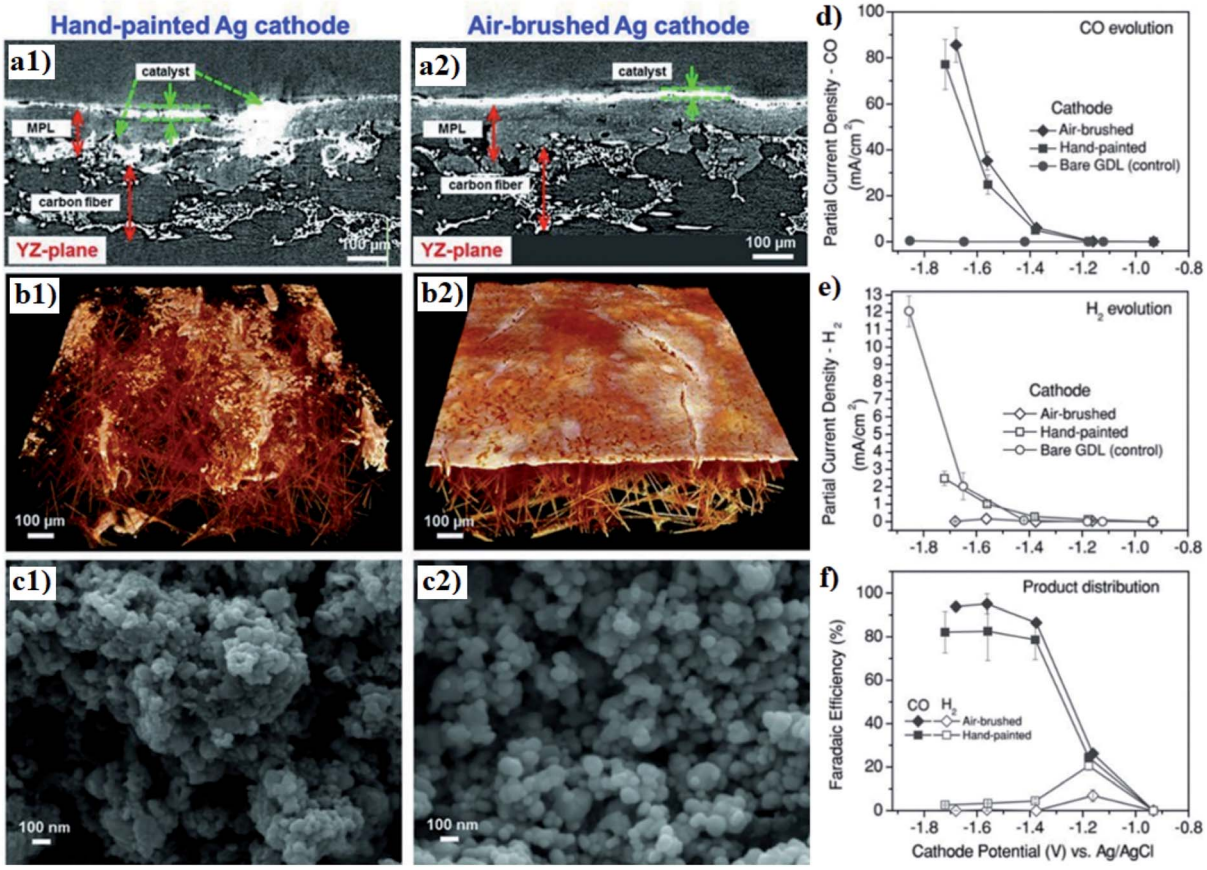

Fig. 13 (a) SEM image of the cross-section (b) MicroCT 3D tomographic virtual models and (c) SEM topography of the Ag GDEs with hand-painted and air-brushed CLs. A comparison of the partial CD of (d) CO and (e) H_2 as well as (f) product distribution for Ag-based GDEs fabricated through hand painting and air brushing. Reprinted with permission from Jhong *et al.*,[193] Copyright 2013, John Wiley and Sons.

the low density of active sites of thin CL could be less significant at high cathodic potential. This mechanism could also partially explain the higher CD of Cu-based GDEs with thin CLs at higher cathodic potentials, as experimentally observed by Sargent *et al.*[45]

In addition to the catalyst loading, the ionic binder also influences the cathode performance. Taking Nafion ionomer for example,[84] it not only forms a continuous matrix in the CL that promotes cation conduction, but also has an impact on the microstructure of the CL that governs CO_2 diffusion. For efficient CO_2 electrocatalysis, therefore, an optimal balance needs to be achieved among the pores for CO_2 diffusion, catalyst particles for electron conduction and catalysis, and ionomer for ion conduction.[179] Through constraining the Sn loading, Zhou and co-workers found that the electrode performance is dependent on the content of the Nafion ionomer, and reported an optimal Nafion loading of 20 wt% in terms of CD and FE.[179] Moreover, the ionomer in the CL can also serve as a co-catalyst promoting the CO_2R reaction. An example is the incorporation of the imidazole-based ionomers to an Sn-based CL could stabilize the $*CO_2^-$ intermediates and therefore enable the electroreduction of CO_2 to HCOOH.[127,191,192]

The dispersion of the catalysts in the CL is another crucial factor for the electrode performance towards CO_2R. Kenis's and

Table 3 Survey of aqueous solutions of inorganic salts-based electrolytes used for electrochemical CO_2R with various operating conditions

Electrolyte	Catalyst	Major CO_2R products (faradaic efficiency, %)	Applied potential (V *vs.* RHE)	Current density (mA cm^{-2})/mass activity (A g^{-1})	Reactor-type[ref.]
0.1 M $KClO_4$	Cu nanowires	C_2H_6 (20.3%)	−1.10	—	H-cell[222]
0.1 M K_2HPO_4		C_2H_6 (10%)			
0.1 M $KHCO_3$		C_2H_6 (17.6%)			
0.1 M $LiHCO_3$	Cu foil	CH_4 (32.2%), C_2H_4 (5.2%), C_2H_5OH (1.6%), $HCOO^-$ (4.7%)	−1.45 (*vs.* SHE)	5	H-cell[223]
0.1 M $NaHCO_3$		CH_4 (55.1%), C_2H_4 (12.9%), C_2H_5OH (4.2%), $HCOO^-$ (7%)	−1.45 (*vs.* SHE)		
0.1 M $KHCO_3$		CH_4 (32%), C_2H_4 (30.3%), C_2H_5OH (10.9%), $HCOO^-$ (8.3%)	−1.39 (*vs.* SHE)		
0.1 M $CsHCO_3$		CH_4 (16.3%), C_2H_4 (30.5%), C_2H_5OH (2.4%), $HCOO^-$ (15.8%)	−1.38 (*vs.* SHE)		
1 M NaCl	Ag-GDE	CO (75%)	−1.87 (*vs.* Ag|AgCl)	72.7 A g^{-1}	Flow-cell[224]
1 M KCl		CO (95.6%)	−1.84 (*vs.* Ag|AgCl)		
1 M RbCl		CO (93.6%)	−1.83 (*vs.* Ag|AgCl)		
1 M CsCl		CO (87%)	−1.81 (*vs.* Ag|AgCl)		
1 M NaBr		CO (60.8%)	−2.33 (*vs.* Ag|AgCl)		
1 M KBr		CO (96.6%)	−1.76 (*vs.* Ag|AgCl)		
1 M RbBr		CO (95.8%)	−1.80 (*vs.* Ag|AgCl)		
1 M CsBr		CO (93.6%)	−1.64 (*vs.* Ag|AgCl)		
1 M NaI		CO (80.8%)	−1.81 (*vs.* Ag|AgCl)		
1 M KI		CO (96.6%)	−1.64 (*vs.* Ag|AgCl)		
1 M RbI		CO (96.5%)	−1.59 (*vs.* Ag|AgCl)		
1 M CsI		CO (101.7%)	−1.56 (*vs.* Ag|AgCl)		
1 M NaOH		CO (83.0%)	−1.86 (*vs.* Ag|AgCl)		
1 M KOH		CO (96.7%)	−1.70 (*vs.* Ag|AgCl)		
1 M RbOH		CO (91.6%)	−1.63 (*vs.* Ag|AgCl)		
1 M CsOH		CO (89.8%)	−1.60 (*vs.* Ag|AgCl)		
3 M $KHCO_3$	Ag-GDE[a]	CO (82.5%)	−0.74	23.1	Flow-cell[225]
3 M KOH		CO (101.5%)	−0.80	234.8	
3 M KCl		CO (73.6%)	−0.81	10.7	
0.1 M $LiHCO_3$	Ag foil	CO (59.1%)	−1.0	1.97	H-cell[62]
0.1 M $NaHCO_3$		CO (68.4%)		2.75	
0.1 M $KHCO_3$		CO (82.9%)		4.06	
0.1 M $RbHCO_3$		CO (82.2%)		4.65	
0.1 M $CsHCO_3$		CO (80.3%)		5.54	
0.1 M $LiHCO_3$	Cu foil	CH_4 (6.2%)		2.40	
0.1 M $NaHCO_3$		CH_4 (17.7%), C_2H_4 (5.5%)		2.57	
0.1 M $KHCO_3$		CH_4 (15.3%), C_2H_4 (10.2%), $HCOO^-$ (4.7%)		3.03	
0.1 M $RbHCO_3$		CH_4 (13.2%), C_2H_4 (24.4%), C_2H_5OH (9.6%)		4.03	
0.1 M $CsHCO_3$		CH_4 (9.4%), C_2H_4 (31.1%), C_2H_5OH (11.4%)		4.80	

[a] GDE means gas diffusion electrodes.

coworkers studied the effects of catalyst dispersion by comparing the performance of Ag-based GDEs prepared using hand painting and air-brushing CL deposition methods.[193] They found that the automated air-brushing technique renders a more uniform catalyst distribution and reduced particle agglomeration in the CL, as shown in Fig. 13a–c, thereby suppressing the HER and promoting the evolution of CO, though the overall CD was not significantly affected by the microstructural difference. They considered such product yield difference to be a result of exposed carbon from MPL that promotes HER, which is evidenced by the observed high HER PCD for bare GDL (Fig. 13d and e); a uniformly dispersed CL could reduce such carbon exposure and therefore suppress the unwanted HER.[193]

5 Electrolyte selection

The primary function of the electrolyte in a CO_2R electrolyzer is to conduct ionic charge between electrodes. An electrolyte generally consists of three components: an inert electrolyte or salt, the solvent (*e.g.* water), and the electroactive species. A good solvent should have (1) a high solubility for the reactant (CO_2) and desired electrolyte to provide conduction; (2) electrochemically stable; (3) be chemically compatible with the electrode materials including the active catalysts; (4) low viscosity if liquid at the cell operating temperature to ensure good rates of CO_2 mass transfer from the bulk electrolyte solution to the electrode surfaces[194,195] and (5) easy to handle, storage, and safe. Water is the most common solvent for CO_2R electrolytes because water satisfies the properties listed above, and can acts as both a proton donor and proton acceptor to facilitate production of different electroactive species.

A key requirement of inert electrolytes commonly used in CO_2R processes is that the electrolyte easily dissociates into cations and anions so as to provide a high ionic conductivity.[196] However, the effect of the electrolyte ions on CO_2R is far more complex than a simple charge carrier relationship.[197,198] Even if the ions of inert electrolytes do not participate directly in redox reactions, an inert electrolyte can affect CO_2R, for example, through interactions of electrolyte ions with radicals and ions produced in the CO_2R reaction as described by Setterfield-Price and Dryfe.[199]

An operational issue common for all types of electrolytes is that impurities in the electrolyte can poison cathode catalysts. For example, trace metal impurities electrodeposited at the cathode during the CO_2R process can lead to loss of CO_2R selectivity with increased relative rates of the HER.[18] Therefore, usually high purity inert electrolytes or electrolyte purification by pre-electrolysis is required. Alternatively, chelating agent such as ethylenediaminetetraacetic acid (EDTA)[19] or a solid-supported iminodiacetate resin (Chelex)[200] could be used to mitigate effects of impurities on CO_2R.

5.1 Aqueous solutions of inorganic salts

The most commonly reported electrolytes for CO_2R are simple aqueous, inorganic salt solutions such as potassium bicarbonate ($KHCO_3$), and some common examples are summarized in Table 3. Although CO_2 solubility in aqueous salt solutions[201,202] may be low as compared to other CO_2 capture solvents such as aqueous amine solutions;[203,204] aqueous salt solutions are widely available at large scale and low cost; are relatively easy to prepare, handle, and store safely; and exhibit stable ionic conductivity.[154,205–207] Since the 1950s the natural gas and ammonia industries have captured CO_2 using the Benfield Process with hot solutions (100–116 °C) of potassium carbonate (K_2CO_3) to capture CO_2 to form $KHCO_3$.[208] It's not surprising that given this long industrial history, $KHCO_3$ solutions have become the most commonly reported aqueous electrolytes for CO_2R.[196,209–217] Carbonates are also chemically compatible with most electrode materials (relative to other conducting salts such as sulfides,[218] sulphates,[219] and halides[190,220,221]). Importantly, bicarbonate solutions provide capacity to buffer the local pH at the electrode surface during CO_2R.[56] The $KHCO_3$ cases described here highlight the complexity of the effects of electrolyte choice in a CO_2 electrolyzer, and to understand these effects more clearly, we discuss separately the roles of cations and anions in aqueous salt electrolytes.

5.1.1 Cationic effects. Many studies report that alkali cations effect CD and product distribution of CO_2R in aqueous electrolytes.[223,224,226,227] Several theories have been proposed to explain these observations, including the specific adsorption of cations or DL blocking by cations,[223] the degree of cation hydration,[62] and stabilization of the negatively charged intermediate ($*CO_2^-$)[224] and related electronic field effects by the cation.[60,228] For example, as shown in Fig. 14, Akira and Hori[223] observed a higher selectivity for C_2H_4 and alcohols over CH_4 and H_2 in electrolytes with larger cations using a series of electrolytes with ionic size increasing from $Li^+ < Na^+ < K^+ < Cs^+$. Hori *et al.*[223] proposed that such cationic effects arise from the tendency of the cations to specifically adsorbed on the electrode surface, which is predominated by the reaction energetics and the hydration capacity of the cation.[224,229] The hydration capacity is stronger for smaller alkali cations,[230] and therefore a Li^+ ion binds more strongly with water molecules than a Cs^+ ion, and

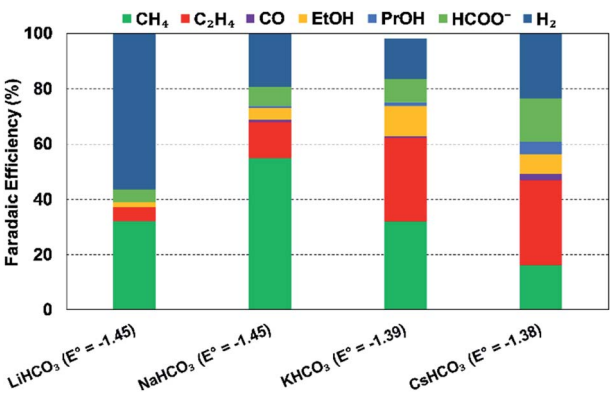

Fig. 14 Effect of cationic species (different 0.1 M bicarbonate solutions) on FEs of various products at a Cu electrode and at 5 mA cm^{-2}; E° values are *vs.* SHE, reproduced from the data in Akira and Hori (1991).[223]

the Li^+ is less likely to adsorb at the cathode surface than Cs^+. Larger cations such as Cs^+ are more readily adsorbed at the electrode surface due to their weaker hydration capacity,[223] which will shift the CO_2 reduction potential towards the positive direction at the outer Helmholtz layer (OHL). This decreased reduction potential will result in a lower proton concentration at the OHL,[223] as suggested by Frumkin as early as 1959.[231] Also, the repulsion between the adsorbed cations and H^+ can further reduce proton concentrations at the electrode surface, therefore contributing to a reduced selectivity towards CH_4 and H_2 as observed by Hori *et al.*[223] (Fig. 14).

Thorson *et al.*[224] proposed that adsorbed cations at the electrode surface could stabilize the intermediate $*CO_2^-$ and thus promote the CO_2R. This theory could explain the observed enhancement in total CO_2R efficiencies with cation size from Li^+ to K^+ (Fig. 14). Recently, Kim *et al.*[232] provided further evidence to support this proposed mechanism by observing an efficient CO production over a Au electrode in K^+-based electrolyte (K^+ is prone to adsorb at the Au electrode) than in a Na^+-based one. Further DFT calculations reported by Liu *et al.*[233] revealed that higher electron-density of adsorbed K^+ close to the carbon atom could facilitate in the stabilization of intermediates such as *COOH and *CO.

However, there remains some debate around the conclusions of Thorson *et al.* For example, Mills *et al.*[234] and Strmcnik *et al.*[235] argued that the specific adsorption of cations seems impossible under the operating conditions for CO_2R (usually for potentials larger than −1.4 V *vs.* a normal hydrogen electrode (NHE, potential defined at 1 M H^+ concentration and 1 atm pressure)). Bell and co-workers proposed that the observed cationic effect originates from the hydrolysis of the solvated cations close to the cathode surface.[62] At the cathode surface,

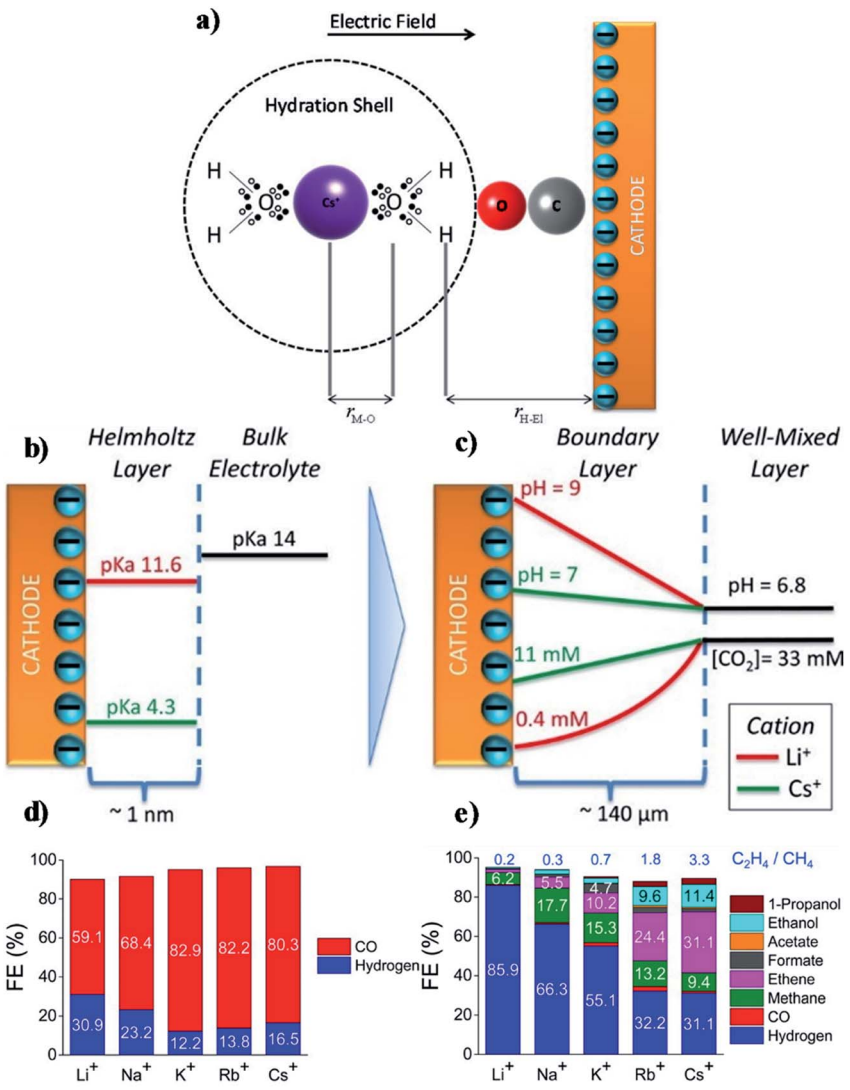

Fig. 15 (a) Interaction of hydrated cation with the negatively charged cathode surface. The additional electrostatic force between the H atom of the H_2O in the primary hydration shell and the cathode causes a decrease in the pK_a of hydrolysis; (b) pK_a of hydrolysis of hydrated Li^+ and Cs^+ inside the Helmholtz layer and in the bulk electrolyte; (c) concentration of CO_2 and pH distribution in the boundary layer; (d and e) FE of different products over Ag and Cu electrodes respectively at −1.0 V *vs.* RHE. The electrolyte was saturated and the concentration was kept at 0.1 M $XHCO_3$ (X = Li, Na, K, Rb, and Cs). Reprinted (adapted) with permission from Singh *et al.*,[62] Copyright 2016, American Chemical Society.

pK_a of hydrolysis decreases significantly due to an increasing electrostatic force between the water molecules in the hydration sphere of cation and negatively charged cathode. These interactions can further polarize O–H bonds of water molecules, and consequently facilitate water dissociation to increase the local proton concentration as illustrated in Fig. 15a. This effect decreases the local pH, which permits an increase of dissolved CO_2 concentration locally that can approach the CO_2 concentration in the bulk electrolyte (Fig. 15b and c). The net effect reported by Singh *et al.*[62] was that switching from Li^+ to Cs^+ in an aqueous electrolyte suppressed HER and significantly promoted CO_2R over Ag cathodes (Fig. 15d) or Cu cathodes (Fig. 15e).

Note that these interpretations of the effects of cation hydrolysis only explain experimental observations at potentials less than −1.1 V *vs.* RHE. The phenomenon of hydrolysis of solvated cations is only applicable when (1) the pH of the electrolyte is close to 7; and (2) the pK_a for cation hydrolysis is close to local pH at the electrode; and (3) the reactant concentration is pH dependent.[62] The hydrolysis of the solvated cations close to the cathode surface does not adequately explain the same cationic effects in CO reduction,[223] because the CO concentration is not pH dependent. Koper *et al.*[236] used density functional theory (DFT) calculations to predict the effect of cations on CO reduction to C_2H_2 at pH close to 13, and found that cations could stabilize intermediates, especially dimers *OCCO and *OCCOH, *via* interactions of oxygen atoms in these intermediates.[236] Moreover, the shift in average reaction energies (for Li^+, Na^+, and Cs^+) of CO to C_1 products is close to that reported by Nørskov and co-workers,[60,61] who showed that the cation-induced local electric effect could alter the free-energy landscape of CO_2R to CO by stabilizing the key reaction intermediates.[236]

Bell along with other JCAP researchers[63] conducted experimental measurements and DFT calculations at low cell potentials, and reported electrostatic interactions between the hydrated cations located at the OHL and the adsorbed reaction intermediates that have high dipole moments (such as *CO, *CO_2, *OCCO) at the cathode surface. Such electrostatic interactions lower the energy required for *CO_2 adsorption (an intermediate for $HCOO^-$) and for C–C dimerization to form *OCCHO or *OCCO (which are the key intermediates for C_2H_4 and C_2H_5OH, respectively).[63] As a consequence, the PCD for H_2 and CH_4 formation are uninfluenced by the cation size, while the PCD for $HCOO^-$, C_2H_4, and C_2H_5OH enhanced with cation size.

In future research, the investigation of monovalent cations for CO_2R should be expanded to multivalent cations. Schizodimou and Kyriacou[237] showed that rates of CO_2R can be accelerated by increasing the size of cations and the surface charge of cations. They demonstrated that the CO_2R rate is almost two-fold higher in electrolyte containing La^{3+} than in electrolytes containing Na^+ at similar operating conditions.

5.1.2 Anionic effects. Two principle explanations are described to explain the impact of anions in an electrolyte on CO_2R:[229,238–241] pH and buffering effects, and specific adsorption of anions at the cathode surface.[225] Hori *et al.*[238,241] studied the effects of pH and reported that the production ratio of C_2H_4/CH_4 varies significantly for different anions in electrolyte: the C_2H_4/CH_4 ratio is higher for K_2SO_4 (4.16) and KCl (3.74) than for $KHCO_3$ (1.02) and K_2HPO_4 (0.11) (Fig. 16). This result was attributed to the inadequate neutralization capacity of the non-buffering K_2SO_4 and KCl, which leads to an increase in local pH, promotes higher hydrocarbons and suppresses CH_4.[238,241] Another interesting feature is the promotion of the HER upon increasing the concentration of the K_2HPO_4 from 0.1 to 0.5 M. This result was attributed to the low pH value at the electrode/electrolyte interface as the concentration of the buffer increases.[229,238] Through varying the anion types of the electrolyte with or without buffering (*e.g.* perchlorate, sulfate, bicarbonate, borate and phosphate), Bell and co-workers[240] found that all the studied anions have negligible effects on evolving pH-independent products, such as CO, $HCOO^-$, C_2H_4 and C_2H_5OH,[242–244] but significantly influence the CDs of H_2 and CH_4, which are highly dependent on pH. In comparison with buffering electrolytes (*i.e.* HPO_4^{2-} and HCO_3^-), the non-buffering electrolytes with ClO_4^- and SO_4^{2-} as anions demonstrated a higher local pH and significantly lower CDs in producing pH-dependent H_2 and CH_4.[240] We discuss the effects of pH on CO_2R in more detail in Section 6 of this review.

The specific adsorption of anions on cathode can also alter the CO_2R activity and selectivity.[190,225,245,246] In particular, the adsorption of halide ions on the electrode surface can alter the electronic structure of the catalysts, and thereby influence the interactions between the electrode surface and intermediates.[190] For example, Varela *et al.* showed that Br^- and Cl^- enhanced CO formation, but I^- facilitated formation of CH_4 instead of CO.[190] Moreover, specifically adsorbed halide anions can suppress proton adsorption and thus prefer CO_2R to HER for a Cu-metal electrode.[246] This can be attributed to the presence of covalent interaction between the halides and Cu electrodes, which facilitates the transfer of electrons from Cu-surface to CO_2.[246] In addition, several studies have reported the changes of morphology of a catalyst's surface in the presence of halide anions, especially *via* oxidation–reduction cycles to promote C_{2+} products over copper catalysts.[66,68,247–249] However, it still remains unclear which anion factor influences CO_2R reaction the most.

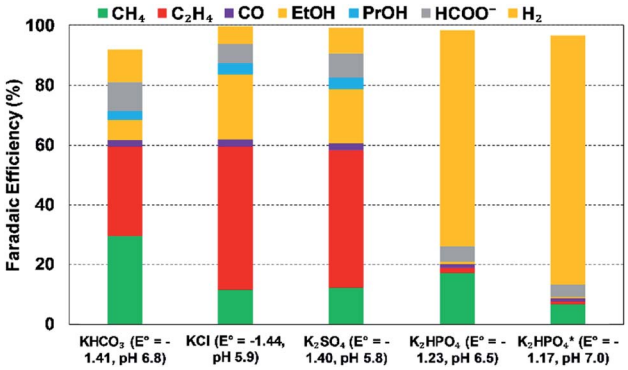

Fig. 16 Effect of anionic species (different 0.1 M bicarbonate solutions) on FEs of various products at a Cu electrode and at 5 mA cm^{-2}; E^o values are *vs.* SHE; *refer to 0.5 M, reproduced from the data in Hori *et al.*[238] (1989).

5.2 Organic solvent electrolytes

Some typical examples of organic solvent electrolytes used for CO_2R are shown in Table 4 with dimethyl sulfoxide (DMSO), dimethylformamide (DMF), propylene carbonate (PC), and acetonitrile (ACN)[250,251] the most commonly reported organic solvents used in CO_2R. The solubility of CO_2 in organic solvents could be much higher than in water (as presented in Fig. 17). As a result of their higher CO_2 solubility and absence of proton, organic solvents can achieve higher CD and better product distribution for CO_2R than in aqueous electrolytes.[27,197,198,229] Vassilev *et al.*[252] reported that DMSO, DMF, PC, and ACN assist in dimerization of $*CO_2$ with adsorbed CO_2 molecules to form oxalate ($C_2O_4^{2-}$) over Pb, In, Sn, and Hg cathodes, which tend to produce $HCOO^-$/HCOOH in aqueous electrolytes.[229] Moreover, the overpotential required to convert CO_2 into products is lower than that in aqueous solution, making the process energy-efficient.[253] Mixed electrolytes containing both organic solvents and water are reported, which allows tuning of proton concentrations.[254] Hori *et al.*[254] found that upon increasing the concentration of water in ACN, CO_2R favors the formation of formic acid rather than oxalic acid.

Although organic solvents offer higher CO_2 solubility than aqueous electrolytes, some critical disadvantages of organic solvent electrolytes are their high cost, their volatility and flammability, and possible toxicity. As the organic solvents are not typically consumed in the CO_2R reaction it could be possible to recycle solvents to reduce the operational costs of CO_2R.[198] However, recycling of organic solvents from the electrolyzer liquid product may be complicated and costly due to the volatility and toxicity of the solvent and potential miscibility with the desired products.[260]

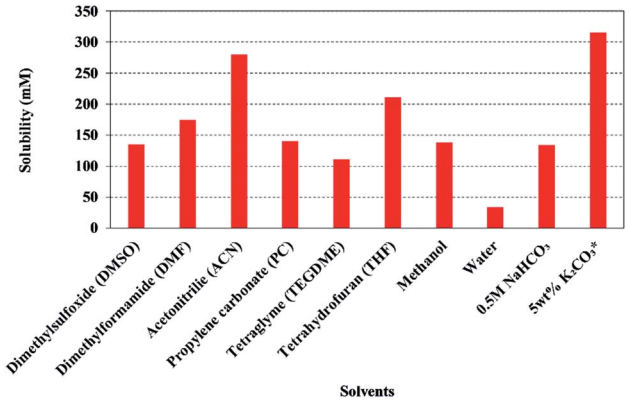

Fig. 17 The solubility of CO_2 in various organic solvents at 298 K and 1 atm.[255–258] *Note: CO_2 solubility in 5 wt% K_2CO_3 was calculated from the CO_2 loading data (0.830 mol CO_2/mol K_2CO_3)[257] and since it includes both chemical and physical CO_2 solubility, therefore, 5 wt% K_2CO_3 has higher CO_2 solubility than organic solvents. Moreover, 5 wt% K_2CO_3 has higher CO_2 loading than 30 wt% aqueous monoethanolamine solution, which is 0.540 (mol CO_2/mol amine) at 298 K and 2.80 kPa (P_{CO_2}).[259]

5.3 Ionic liquids

Ionic liquids (IL) have been proposed as alternatives to aqueous amines for CO_2 capture process[264] because ILs exhibit high CO_2 solubility[265] and high selectivity for CO_2 over other gases such as N_2, O_2, and CH_4.[266] Ionic liquids also exhibit other desirable properties for CO_2R electrolytes such as excellent thermal stability,[267,268] stability across a wide electrochemical potential window,[268,269] high ionic conductivity,[268] and low vapor pressure.[268,270] In addition, some ILs can form a complex with the intermediates during CO_2R and thus lower the energy barrier of the reaction.[191] Table 5 provides a summary of some ILs reported as CO_2R electrolytes. The most extensively studied ILs for use in CO_2R electrolyzers are two commercially available ILs: 1-ethyl-3-methylimidazolium tetrafluoroborate ([EMIM][BF_4]), and 1-butyl-3-methylimidazolium tetrafluoroborate ([BMIM][BF_4]).[191,271,272]

In 2011, Rosen *et al.*[191] first reported the catalytic effect of an 18 mol% aqueous solution of ([EMIM][BF_4]) in the CO_2R to CO over an Ag electrode at low overpotentials to achieve FE_{CO} of over 96%. Fig. 18 illustrates Rosen *et al.*'s[191] hypothesis that an IL cation can stabilize the $*CO_2$ intermediate, and therefore substantially lower the energy barrier for the formation of $*CO_2$ and its subsequent reduction to CO.[191,273,274] Subsequently, the Rosen's team investigated the effect of water on CO_2R in ([EMIM][BF_4]) solutions and found that addition of water in the IL enhanced the CO selectivity, with an optimal CO selectivity

Table 4 Survey of organic solvent electrolytes used for electrochemical CO_2R with various operating conditions

Electrolyte	Catalyst	Major CO_2R products (faradaic efficiency, %)	Applied potential (V *vs.* RHE)	Current density (mA cm^{-2})	Reactor-type[ref.]
0.1 M TBAP/PC	Au foil	CO (91.8%)	−3.02 (*vs.* Fc/Fc^+)	2.8	H-cell[260]
0.1 M TEAP/PC	Pb foil	$H_2C_2O_4$ (73.3%)	−2.4 (*vs.* SHE)	—	H-cell[250]
0.1 M TEAP/PC	In foil	CO (85.3%)			
DMF	Pb foil	CO (n.a.)	—	—	H-cell[251]
0.5 M LiCl/methanol	Cu foil[a]	CO (~65%), CH_4 (20%)	−2.8 (*vs.* SHE)	15	H-cell[261]
0.08 M CsOH/methanol	Cu foil	CH_4 (8.3%), C_2H_4 (23.7%)	−4.0 (*vs.* Ag|AgCl)	—	H-cell[262]
0.08 M benzalkonium/methanol	Cu foil[b]	CO (~7%), CH_4 (42.5%), C_2H_4 (2.1%)	−2.0 (*vs.* SCE)	—	H-cell[263]

[a] At high pressure (10 atm). [b] At low temperature (−30 °C); PC – propylene carbonate; TBAP – tetrabutylammonium perchlorate; TEAP – tetraethylammonium perchlorate; DMF – dimethylformamide; LiCl – lithium chloride; CsOH – cesium hydroxide.

Table 5 Survey of Ionic liquids (ILs) as electrolytes used for electrochemical CO_2R with various operating conditions[a]

Electrolyte	Catalyst	Major CO_2R products (faradaic efficiency, %)	Applied potential (V *vs.* RHE)	Current density (mA cm^{-2})	Reactor-type[ref.]
18 mol% [EMIM][BF_4]/water	Ag-GDE	CO (~96%)	1.5 to 2.5 V (cell potential)	—	Flow-cell[191]
[EMIM][BF_4]	Ag NPs (40–200 nm) onto Sigracet carbon paper (5 mg cm^{-2})	CO (—)	3.25 V (cell potential)	4	Flow-cell
0.02 M [EMIM][BF_4]/0.1 M [TBA][PF_6]/ACN	Bi electrodeposited onto a glassy carbon electrode	CO (93 ± 7%)	−1.95 (V *vs.* SCE)	~3.77	H-cell[279]
0.02 M [BMIM][BF_4]/0.1 M [TBA][PF_6]/ACN		CO (95 ± 6%)		~5.51	
0.02 M [BMIM][PF_6]/0.1 M [TBA][PF_6]/ACN		CO (90 ± 9%)		~4.82	
0.02 M [BMMIM][BF_4]/0.1 M [TBA][PF_6]/ACN		CO (76 ± 6%)		~0.67	
80 wt% [BMIM][Cl]/water	Ag foil	CO (>99%)	−1.5 (V *vs.* SCE)	—	H-cell[271]
4 mol% [EMIM][BF_4]/water	Bulk MoS_2	CO (~98%)	−0.764	65	H-cell[275]
0.1 M[EMIM][NTf_2]/ACN					
0.02 M [DMPIM][BF_4]/0.1 M [TBA][PF_6]/ACN	Ag foil	CO (~100%)	−1.48 (V *vs.* Fc/Fc^+)	4.2	H-cell[282]
0.5 M [EMIM][$N(CN_2)$]	Sn NPS/glassy carbon	$HCOO^-$ (81.9%)	−1.2	~4.18	H-cell[283]
0.1 M [TBA][PF_6]/ACN	Ag foil	CO (74%)	−2.1 (V *vs.* SCE)	17	H-cell[284]
0.5 M [BMIM][PF_6]/0.1 M [TBA][PF_6]/ACN		CO (97%)		50	
[BMIM][PF_6]	Pb foil	CO (~100%)	−2.2 (V *vs.* $Ag|Ag^+$)	0.33	H-cell[285]
30 wt% [BMIM][PF_6]/ACN		HCOOH (46.3%), CO (40.2%)		2.63	
30 wt% [BMIM][PF_6]/5 wt% water/ACN	Pb foil	HCOOH (91.6%)	−2.3 (V *vs.* $Ag|Ag^+$)	37.6	
30 wt% [BMIM][PF_6]/5 wt% water/ACN	Sn foil	HCOOH (92%)		32.1	

[a] [EMIM] – 1-ethyl-3-methylimidazolium; [BMIM] – 1-butyl-3-methylimidazolium; [TBA] – tetrabutylammonium; [BMMIM] – 1-butyl-2,3-dimethylimidazolium; [DMPIM] – 1,3-dimethyl-2-phenyl-imidazolium; [BF_4] – tetrafluoroborate; [PF_6] – hexafluorophosphate; [NTF_2] – bis(trifluoromethylsulfonyl)imide; [CN_2] – dicyanamide; ACN – acetonitrile.

close to 100% in a solution of 10.5 mol% IL in water. Such performance enhancement was attributed to a synergistic effect of mass-transfer improvement due to lower the electrolyte's viscosity by dilution with water and an optimal pH (pH around 3.2 at 89.5% water).[274]

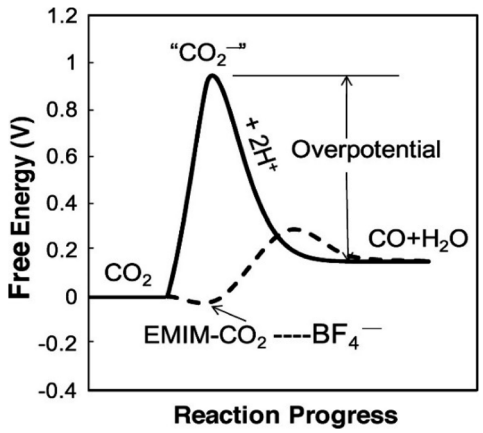

Fig. 18 A change in free energy of CO_2 to CO in water (solid line) to CO_2 to CO in EMIM-BF_4 (dashed line). Reprinted with permission from Rosen *et al.*,[191] Copyright 2011, American Association for the Advancement of Science.

Following Rosen *et al.*'s work,[191] others have attempted to understand the catalytic effect of the ILs in CO_2R, and although there is still more to understand about the reaction mechanism most reports suggest that the cation is primarily responsible for the observed catalytic effects.[271,275–278] For example, Rosenthal and co-workers proposed that ILs serve as a proton source by investigating the catalytic performance of the Bi-based catalyst in AN solutions of $[BMIM]^+$-based ILs.[279,280] Deprotonation from the C_2 position (refer to Fig. 19) of the $[EMIM]^+$ or $[BMIM]^+$ cation would result in the conversion of CO_2 to CO *via* the $2e^-/2H^+$ reduction pathway, which has a lower energy barrier.[279,281,282]

Despite the many promising properties of ILs for CO_2R electrolytes, the high viscosity of ILs can severely limit the rates of CO_2 diffusion, and thus ILs achieve very low CDs[272] and, as shown in Table 5, most CO_2R studies dilute ILs in aqueous solutions or organic solvents such as AN, DMF, or CH_3OH to reduce the electrolyte's viscosity.[191,271,275,277] Progress in development and application of ILs has progressed rapidly in the last 30 years to provide a large amount of fundamental

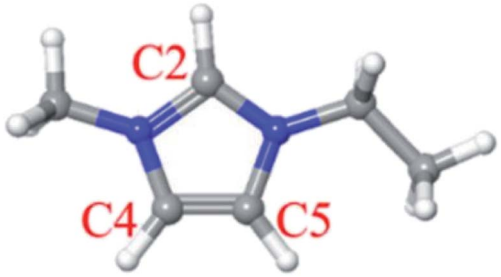

Fig. 19 Structure of imidazolium cation; white is H_2, grey is C and blue is N_2. Reprinted (adapted) with permission from Lau *et al.*,[282] Copyright 2016, American Chemical Society.

understanding of IL properties and physicochemical data, and to lower IL production costs significantly. Thus, ILs are becoming more available and could soon be viable options for use in CO_2R electrolyzers.

6 pH effects

The pH of the electrolyte affects the phase stability of CO_2 in aqueous solutions as illustrated by the Pourbaix diagram in Fig. 20.[229] The Pourbaix diagram highlights the acid/base homogeneous interactions of CO_2 into different forms, such as carbonic acid (H_2CO_3), bicarbonate (HCO_3^-), carbonate (CO_3^{2-}) and methanol (CH_3OH) in water as a function of pH and potential. reaction (6) shows that the introduction of CO_2 into an aqueous solution entails a complex series of reversible reactions between CO_2, water, carboxylic acid, and its deprotonated species. In solutions with a pH up to about 6, CO_2 is in the form of a weak carboxylic acid; at pH between 6 and 10.3, HCO_3^- anions are formed; and at pH above 10.3 HCO_3^- deprotonates further to CO_3^{2-} (reaction (7)). Due to the various reactions and the feed CO_2, most aqueous solutions are normally in the HCO_3^- form and around pH 9 unless specific measures are used to counteract them (*e.g.*, high flow rates).[45]

$$CO_2 \xleftrightarrow{H_2O} CO_{2(aq)} \leftrightarrow H_2CO_{3(aq)} \leftrightarrow HCO_{3(aq)}^- + H_3O^+ \quad (6)$$

$$HCO_{3(aq)}^- \xleftrightarrow{H_2O} CO_{3(aq)}^{2-} + H_3O^+ \quad (7)$$

Note that the local pH near the cathode surface is usually different to that in the bulk electrolyte due to the catalytic reactions generating OH^- or consuming H^+, and diffusion limitations.[287] Despite the significance of local pH on CO_2R as discussed in Hori's works,[229,238,239] only recently has the influence of local pH been re-re-examined.[55,287–292] Additionally, some electrolytes, such as bicarbonates provide pH buffering effects (see Section 5.1.2 for more details).[240]

As the major competing side reaction, HER needs to be minimized for an optimal CO_2R reaction. Therefore, pH is crucial in determining the HER activity, as it characterizes the availability of the protons. Although CO_2R produces OH^-, its equilibrium potential is not much influenced by the pH in comparison to HER.[286] A rise in pH moves the equilibrium potential of HER to a more negative value, thus significantly slowing down HER.[293] As shown in Fig. 21, the equilibrium potential denoted by E_{rev} reflects the potential of the HER derived from the Nernst equation. Moreover, the mechanism of HER switches from protons-to-H_2 in acidic media to water-to-H_2 in alkaline media, where the kinetics of latter is significantly slower and does not have a pH dependence, although the concentration is typically much greater.[294–297]

The pH is also an essential factor in determining the products of CO_2R. Taking Cu as an example, an increase of pH shifts the product selectivity from H_2 and CH_4 to higher carbon products such as C_2H_4.[45,238,241,298,299] The HER suppression at higher pH can be easily described by the reduced availability of H^+/H_{ads}. However, how pH affects CO_2R products (*i.e.* CH_4 preferred at low pH and C_2H_4 at higher pH) is very complex, and is likely related to the multiple proton-coupled-electron steps involved in their various reaction pathways, and the rate-determining steps in those various microkinetics.[294,298,300–302]

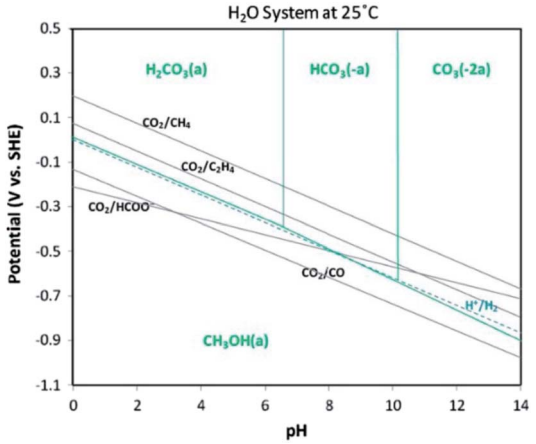

Fig. 20 Pourbaix diagram for electrochemical CO_2R at 25 °C. Reprinted with permission from Ganesh,[286] Copyright 2014, Elsevier Ltd.

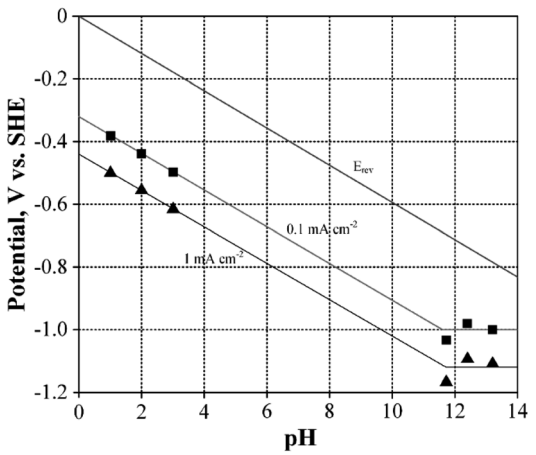

Fig. 21 Hydrogen evolution polarization data at copper (Cu) with varying solution pHs. Reprinted with permission from Gattrell *et al.*,[293] Copyright 2006, Elsevier Ltd.

The different onset potentials[238,299,303] and Tafel slopes[304–306] for CH_4 and C_2H_4 evolution suggest that they follow different reaction pathways. Hori and co-workers proposed that C_2H_4 evolution is pH independent, while the pathway for CH_4 evolution is pH-dependent, during or prior to the rate-determining step (RDS).[306] By using online electrochemical mass spectrometry (OLEMS), however, Schouten's group found that the onset potential for forming CH_4 and C_2H_4 are both pH-dependent particularly over Cu (111) electrode.[307,308] Schouten and co-workers proposed two possible reaction pathways for the formation of C_2H_4 as illustrated in Fig. 22a. One pathway is pH-independent, involving the formation of CO dimer where proton transfer is not the RDS, and preferentially takes place at Cu (100) facets. This pathway has also been theoretically confirmed by Calle-Vallejo and Koper.[309] Another pathway is pH dependent, sharing the same *CHO intermediate, which is also critical in evolving CH_4, and takes place both at Cu (100) and (111) facets. More interestingly, the overpotential for both CH_4 and H_2 evolution is lowered at a very high pH (*e.g.* pH = 13, see Fig. 22b).[308,310] The reduced overpotential of HER at higher pH could be a result of the possible reaction pathway shift from pH dependent (due to proton availability) to pH independent (due to water discharge).[293,311] Likewise, it could be understood that a similar shift likely takes place during the formation of the CH_4 at higher pH. Based on this understanding, electrolytes with higher pH can favor the formation of higher hydrocarbon products (especially over copper catalysts). Recently, Sargent and co-workers[45] showed that strong alkaline media (7 M KOH) accelerates the kinetics of CO_2R by lowering the C–C coupling energy barrier over Cu catalyst and could achieve a C_2H_4 FE of ~70% at −0.55 V *vs.* RHE over 150 h of continuous CO_2R operation. Therefore, more researchers are investigating KOH as electrolyte to further enhance the efficiency and selectivity of $>C_2$ products.[45,312]

Additionally, it could be understood that a rise in the local pH could be beneficial for $>C_2$ products; however, with a rise in local pH, the equilibrium of CO_2 and water neutralization reaction shifts more towards bicarbonate formation, which eventually depletes the local CO_2 concentration and thus reduces the CO_2R selectivity by promoting HER.[62,290] This conflicting statement really begs a question on whether a high local pH is really desirable or deleterious for the CO_2R reaction. At higher pH, CO_2 may still exist in low quantity (if ample CO_2 is transported into the solution) due to its limited hydration kinetics.[242,313] Therefore, an optimal pH may exist for an efficient reaction and sufficient CO_2 supply. Recent modeling studies found a relationship between pH and selectivity of CO_2R with a maximum CO_2 selectivity over an optimal local pH range of 9 to 10 (especially for C_2 products).[154,314] Interestingly, at higher pH, the selectivity and activity of $>C_2$ products reach a maximum and finally start decreasing, whereas, CH_4 evolution starts increasing.[63] A possible reason for this behavior could be the increased coverage of H* caused by the depletion of CO* in the limited mass-transport regime. Such adsorbed protons promote CH_4 evolution (by CO hydrogenation) and reduce the chances of CO* coupling to make $>C_2$ products.[315,316]

Furthermore, in a relatively alkaline environment, the Cannizzaro reaction (Fig. 23a) could take place during CO_2 electrolysis. In a Cannizzaro reaction, an aldehyde can disproportionate to the corresponding carboxylic acid and alcohol.[317] Through investigating the reduction of formaldehyde in various electrolytes, such as perchloric acid ($HClO_4$), sodium perchlorate ($NaClO_4$), and phosphate buffers, Koper and co-workers observed that the disproportionation reactions are strongly influenced by the electrolyte pH and buffering strength.[317] As OH^- ions are essential for the Cannizzaro reaction, HCOOH is easier to form in the $HClO_4$-based electrolyte (pH = 3) than the one with pH = 1 (see Fig. 23b). In phosphate electrolyte with a high buffering capacity and thereby a relatively low local pH, Cannizzaro reaction was significantly hindered, leading to a negligible formation of HCOOH.[317] Therefore, researchers should be careful in distinguishing the products such as acids and alcohols formed from the disproportionation reactions and those formed by direct CO_2R, especially for the liquid products such as methanol and ethanol, where the corresponding aldehyde is often proposed as a reaction intermediate.[318] This is especially true since interrogation of the just produced products is hard to measure compared to

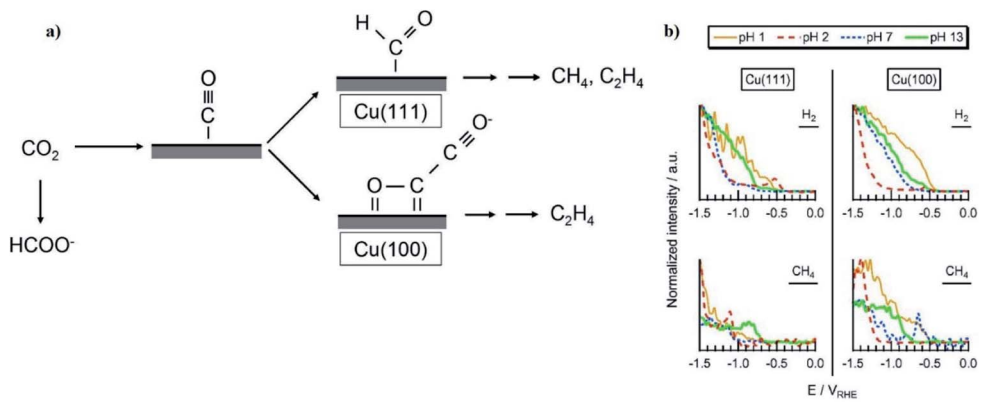

Fig. 22 (a) The proposed reaction mechanism for the reduction of CO_2 on Cu single crystal electrodes and (b) the reduction of CO in 0.1 M $HClO_4$ (pH 1), 0.2 M $NaClO_4$ (pH: 2 and 7) and 0.1 M NaOH (pH: 13) on Cu (111) left and Cu (100) right. Reprinted with permission from Schouten *et al.*,[308] Copyright 2014, Elsevier Ltd.

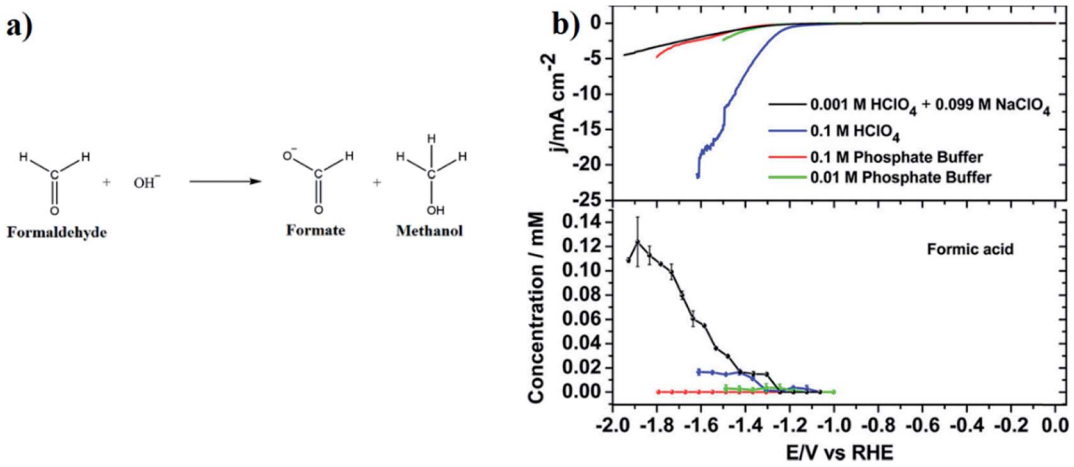

Fig. 23 (a) Cannizzaro disproportionation reactions showing formaldehyde disproportionate to formate and methanol, adapted from Birdja and Koper[317] (2017), (b) formic acid formation during reduction of formaldehyde in perchloric acid (pH: 1 and 3), 0.1 M phosphate buffer pH 6.6, and 0.01 M phosphate buffer pH 6.8. Scan rate: 1 mV s^{-1}. Reprinted with permission from Birdja and Koper,[317] Copyright 2017, American Chemical Society.

the ones that further react and transport and are detected in the bulk solution or gas flows.

Enhanced mass transport makes the value of local pH closer to the bulk pH, thus influencing the activity and selectivity of cathodic reactions.[295,319] Through rotating a Cu cylinder electrode to enhance the mass transfer, Marshall and co-workers found that the CO_2R activity decreased with the increasing rotation speed, along with a change in product preference from CH_4 to CO, while HER was promoted.[319] Such degradation of CO_2R is attributed to the formation of graphitic carbon on electrode surface due to low local pH at higher rotation speed, resulting in the deactivation of the active sites for CO_2R.[319] This evidence is also supported by Mul and co-workers, who presented a pH-dependent pathway for the deactivation of Cu electrode due to carbon formation.[288] In addition, the change in product selectivity from CH_4 to CO at higher rotation speed could be due to lower coverage of adsorbed *CO, which is a precursor for CH_4 formation.[319]

7 Pressure and temperature effects

7.1 Pressure

The partial pressure of CO_2 in the gas fed to the electrolyzer directly impacts the rate of CO_2 mass transfer to the electrode surface due CO_2-solvent solubility relationship. For example, at a given temperature CO_2 solubility in aqueous electrolytes and physical organic solvents typically increases linearly with pressure according to Henry's law.[320] Other solvent-electrolytes like amines[321] and ILs[322] exhibit non-linear CO_2 solubility relationships that may reach a plateau at a critical pressure (*e.g.* around 10 MPa for imidazolium-based ionic liquids[322] and ~1 MPa for amines[323]) beyond which further increase of pressure does not improve solubility. Raising the operating pressure increases complexity and cost of electrolyzer construction and operation, so optimization of the pressure must consider costs and the effect of pressure on CO_2R selectivity.

A large number of studies report the effects of pressure on product selectivity and FE of CO_2R processes.[67,108,109,159,210,212,288,324–330] Hara *et al.*[330] reported that on a Cu wire (0.16 cm^2) in 0.1 M $KHCO_3$ the CO_2R products shifted from H_2 at 1 atm to hydrocarbons then to CO and/or HCOOH as the pressure was increased to 30 atm, with PCD_{CO} up to 523 mA cm^{-2} observed. Table 6 summarizes a typical example reported by Hori *et al.*[210] of the effect of CO_2 pressure on product selectivity over different metal electrodes. Hori *et al.* observed that over group B catalysts, which include Fischer–Tropsch catalysts like Ni, Co and Fe, product selectivity shifted from H_2 at ambient pressures to HCOOH and CO at high pressure.[210] Kudo *et al.*[331] reported similar shifts from H_2 at low pressures to CO, HCOOH, and hydrocarbons at 60 atm over Ni catalysts as shown in Fig. 24a. They observed that the hydrocarbons from CO_2R over Ni followed a Schulz–Flory probability distribution like that obtained by the Fischer–Tropsch reaction, and proposed that like the conventional Fischer–Tropsch process electrochemical CO_2R at high pressures may involve hydrogenation of metal

Table 6 Effect of pressure on the product distribution of different metal electrodes in an electrochemical CO_2R process, data was taken from Hara *et al.*[210] (1995)

		Effect of pressure	
Group	Cathode catalyst	Major products at 1 atm	Major products at 30 atm
A	Ti, Nb, Ta, Mo, Mn, and Al	H_2	H_2
B	Zr, Cr, W, Fe, co, Rh, ir, Ni, Pd, Pt, C and Si	H_2	CO and HCOOH
C	Ag, Au, Zn, In, Sn, Pb, and Bi	CO and HCOOH	CO and HCOOH
D	Cu	CH_4 and C_2H_6	CO and HCOOH

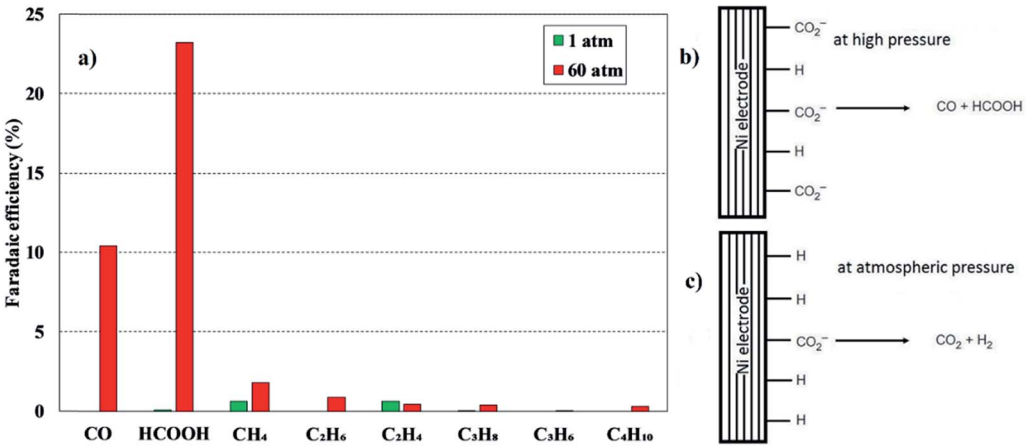

Fig. 24 Electrochemical reduction of CO_2 on Ni electrodes, (a) effect of pressure on the FE of various products; reaction mechanism (b) at high pressure (60 atm), and (c) at atmospheric pressure. Adapted with permission from Kudo *et al.*[331] Copyright 1993, The Electrochemical Society.

carbonyl intermediates to facilitate production of carbene groups (–CH_2–) that polymerize to longer-chain hydrocarbons. In addition, high CO_2 pressure increases the surface coverage of CO_2R intermediates on the electrode surface, which promotes CO_2R and suppresses of HER as illustrated in Fig. 24b and c.[210,331]

For group C catalysts like Ag and Sn, Hara *et al.*[210] did not report a major shift in the type of CO_2R products at higher pressure but the FE towards CO and HCOOH did increase (relative to H_2), and this was attributed to increased CO_2 solubility at higher pressures. Over Cu catalysts (group D), Hara *et al.*[210] reported a shift from hydrocarbon production at 1 atm to CO and HCOOH at 30 atm. Jesús-Cardona *et al.*[326] proposed that at concentrations of CO_2 in the electrolyte at elevated pressure, CO_2 molecules displace may displace at the electrode's surface some of the CO* that are a key intermediate in the CO_2R to hydrocarbon pathway.

High-pressure CO_2R requires balancing the pressure in the anode and cathode chambers to prevent damage to the separator.[98,212,262] Ramdin *et al.*[98] compared the effects of BPM and CEM on CO_2R to formic acid/formate at high CO_2 pressure, and after the experiment observed delamination of BPM layers. Note that even in electrolyzer operating at near ambient pressures there can be a pressure imbalance across the separator, especially in CO_2R processes where the anode produces O_2 and the cathode reduces CO_2 to liquid products. This pressure imbalance can deform the separator, so to improve mechanical strength thicker membranes, fabric-reinforced membranes, or additional porous substrates may be require. These approaches may improve strength and durability, but also increase the resistances across the separator.[332]

7.2 Temperature

Temperature effects CO_2R electrolyzer performance because of both CO_2 solubility (*i.e.* the Van't Hoff equation)[333,334] and minimum half-cell potentials are temperature dependent, and temperature influences CO_2R kinetics because of its effect on mass transfer rates, reaction pathways, viscosity and conductivity of electrolytes, and the conductivity of IEM separators. The stability of cell components like membranes, electrodes, and gaskets may also be effected by temperature extremes or by temperature cycles. The range of temperatures reported for electrochemical CO_2R processes is commonly between 20–40 °C, although a few studies have explored CO_2R at temperatures as low as 0 °C (ref. 209) and up to 125 °C.[54] Within this operating range the temperature dependency of electrical conductivity of cell components like current collectors is unlikely to have a significant effect on CO_2R electrolyzer performance.

The main CO_2R reactions and the HER have a positive entropy change so that lower overall thermodynamic cell voltages are required for reactions at higher temperatures. Additionally, lower activation overpotential are required at higher temperatures than lower temperatures to drive a sufficient overall CO_2R rate, which can be quantitatively determined through the Butler–Volmer equation.[335] The effect of temperature on overpotential appears to be more significant than the effect on thermodynamic potentials. For example, Dufek *et al.* reported a significant reduction of cathode potentials from −2.19 V to −1.87 V to achieve 70 mA cm^{-2} over an Ag-based GDEs when operating temperature was elevated from 18 to 70 °C, while less than 0.1 V decrement in thermodynamic voltage was observed when the temperature was increased from 25 to 125 °C.[54] Ryu *et al.*[336] reported a similar trend for CO_2R over Hg electrodes.

Temperature has a significant effect on hydrodynamic properties (viscosity and density) and concentration gradients (due to solubility relationships) that control rates of CO_2 mass transfer. For example, faster CO_2 mass transfer coefficients from the gas to electrolyte is observed at higher temperatures because diffusivity of CO_2 in gas and liquid phases increases, and the viscosity of the catholyte decreases.[337,338] But, a reduced solubility at higher temperatures lowers the overall driving force for the mass-transport across the gas/liquid interface. The relative changes in solubility with temperature for CO_2 compared to CO_2R products such as CH_4 and C_2H_4 that are

sparingly soluble in the catholyte,[339,340] could be advantageous to promote quick desorption of products from the electrode surface. However, proton transfer rates may also increase at high temperatures and so increasing temperature can potentially promote HER at the cathode.

The enhanced diffusivity and thinner static laminar layer at the electrode exhibited at higher temperatures reduces ohmic resistances in the electrolyte. In GDEs, temperature can also change the phase-change induced flow and result in dryers CLs.[189] However, increased temperature means higher water entering into the electrolyzer at same relative humidity and so that can help get to higher CDs, especially if the system is water limited.[189]

Temperature is known to affect the product distribution of the CO_2R reaction over different catalysts.[341–344] for example, Hori *et al.*[209] reported a decrease of FE_{CH_4} and increase of $FE_{C_2H_4}$ over Cu foil at 5 mA cm^{-2} when the temperature was raised from 0 to 40 °C. Ahn *et al.*[343] reported a similar trend when increasing the temperature from 2 to 22 °C. A close proximity of *CO intermediates is important for the formation of C–C bond, meaning that a high *CO coverage should make it easier for the C_2H_4 evolution. However, the reported suppression of C_2H_4 at high temperature, where the coverage of *CO is low, suggests that *CO coverage may not play a dominating role at least within the studied range. Alternatively, several recent theoretical studies proposed that *COH and *CHO intermediates are crucial to determine whether the product is CH_4 or C_2H_4, respectively with a Cu electrode.[318,345,346] According to the work reported by Luo *et al.*,[346] the availability of absorbed protons is essential to form *CHO, while the absorbed H_2O is important to serve as a shuttle ($H_3O^{\delta+}$) to transfer the proton to the *CO intermediate to form *COH. Therefore, one possible explanation of the reported temperature effect is that low temperature can stabilize the formation of ($H_3O^{\delta+}$) proton shuttle, making it easier to form *COH intermediate, thus facilitating the production of CH_4. On the other hand, higher temperatures increase the availability of adsorbed protons at the electrode surface, resulting in an easier formation of *CHO intermediates that promote C_2H_4. Moreover, the adsorbed protons could also partially contribute towards promoting HER. When temperature further increased from 22 °C, a degraded FE(C_2H_4) over Cu electrode was observed by Ahn *et al.*[343] This suggests that the aforementioned coverage of *CO starts to dominate instead of the coverage of adsorbed protons.[343] Interestingly, potential *vs.* RHE showed an opposite trend when comparing the temperature-effect results reported by Hori *et al.* and Ahn *et al.* Nevertheless, both studies report similar observations towards FE of CH_4 and C_2H_4, suggesting that the potential effect as imparted by the temperature change on the product distribution could be negligible in the studied temperature range.

Considering the effects of the potential on the reactivity and selectivity as mentioned, we recommend the design of experiment to keep the potential *vs.* RHE constant when investigating temperature effects, as this potential is corrected by both temperature and pH. Overall, the temperature has significant impacts on the surface coverage of CO_2R-related species (*COOH and *CO) through affecting their mass-transfer characteristics (*e.g.* solubility), as well as the coverage of proton-related adsorbates (*e.g.* H* and $H_3O^{\delta+}$) that also are important for the formation of key intermediates (*e.g.* *CHO and *COH). Such effects likely contribute the observed temperature-dependent CO_2R selectivity.

A small increase in temperature can lower the ohmic resistance of the separator.[94,347] However, too high of a temperature degrades the ionic conductivity and mechanical structure of the membranes. Taking perfluorosulfonic acid (PFSA) polymer-based membrane as an example, its clusters of the hydrophilic sulfonic-acid group uptake sufficient water and allow protons to move easily in the membrane. In a fuel-cell configuration, a too high temperature (>90 °C) lowers the water content in the membrane, leading to a decreased ionic conductivity.[348] Common AEMs, such as quaternary ammonia polysulfone, limit the operation to a much lower temperature than CEMs due to chemical stability concerns.[349] The Sustainion® membrane, developed by Dioxide Materials, has an improved ionic conductivity (~140 mS cm^{-1} in 1 M KOH aqueous solution at 80 °C) and can stably be operated at temperature up to 80 °C.[347] Ceramic based separators such as ZrO_2 diaphragm can withstand higher operating temperature, but again they also pose other key risks such as product crossover that lose conversion efficiency of the cells.

8 Summary and outlook

We have examined in this review the impact of design and operating decision related to electrolyzer configurations, electrode structure, electrolyte selection, pH, pressure, and temperature affect the reaction conditions at catalyst sites in a CO_2R electrolyzer, and thus impact on the overall efficiency of the process. The key challenges for low cost CO_2R that can be addressed by these factors together with catalyst materials are reducing the required cell voltages, improving selectivity, and lowering product separation costs.

The most promising CO_2R electrolyzers under development are based on designs and understanding translated from polymer electrolyte fuel-cells. Of the types of continuous CO_2R electrolyzers under development, vapor-fed electrolyzers may be the most promising for the large-scale CO_2R processes because this configuration provides opportunity to feed wet CO_2-rich flue gas directly to the electrolyzer without CO_2 capture process units.[350] This technology if coupled with renewable electricity generation could also provide opportunities for passive CO_2 capture from the atmosphere.[351] Vapor-fed electrolyzers may also reduce risks of catalyst poisoning from trace impurities in liquid electrolytes. For large-area electrodes in industrial scale electrolyzers, achieving uniform current and voltage distribution throughout the electrode surface and managing pressure gradients at the gas–electrolyte interface are critical, thus further work is required to optimize the electrode and flow-field design. In this regard, advanced manufacturing technologies like 3D printing[352] combined with computational modelling may help to optimize electrode and electrolyzer geometries.

There are fundamental aspects of electrolyte interactions in CO_2R processes that are not fully understood. For example, although the charge carrying capacity of electrolytes is the

primary function, researchers have discovered that electrolyte cations contribute in other ways to effect to the availability of protons and to stabilize CO_2R intermediates. Likewise, electrolyte anions can provide local pH buffering effects due to specific adsorption of anions at the cathode surface. Low CO_2 solubility and competitive HER remain major challenges in inorganic salts-based aqueous electrolytes. Other new solvent-electrolytes such as ionic liquids and deep eutectic solvents may become more attractive if their cost reduces in the future, but to be effective CO_2R electrolytes the viscosity of these solvents will also need to be managed, for example by mixing with a co-solvent such as water.

While our review has focused on electrochemical CO_2R at the cathode, we acknowledge that the anode catalyst is also critical and especially because the state-of-the-art Ru and Ir based anode materials are a major contributor to the cost of electrochemical CO_2R. Therefore, any advances in anode technologies achieved in other applications such as the oxygen evolution reaction in water splitting should help inform development of electrochemical CO_2R processes. Water purification from treating wastewater through anodic oxidation of organic pollutants could be another approach to be considered for coupling with CO_2R.[353] Moreover, since the oxidation potential of chloride is similar to that of water, producing chlorine at anode[354,355] (similar to chlor-alkali cells) without the expense of extra energy could be beneficial for optimizing the overall process.

A final consideration in research needs for CO_2R relates to experimental methods used to test novel catalysts and electrolyes. Most laboratory studies still use H-type batch setups[40] in which the solubility of CO_2 in electrolyte and gas–liquid mass transfer limits can control the overall rate of CO_2R reactions, plus the transport of ions across separators in H-type cells can limit applicability of long term stability tests. Lab scale continuous flow-cell electrolyzers offer opportunities to detect minor CO_2R products[99] and to better control reaction conditions than in H-cells. The cost of flow-cell apparatus is no longer significantly higher than a batch cells, so we expect the trend in reporting continuous CO_2R measurements in catalyst studies may become more common. Clark *et al.*[200] have also highlighted the urgent need for standardized protocols, such as those developed for battery testing and fuel cell performance, to benchmark performance of catalyst and electrolyzers for electrochemical CO_2.

Conflicts of interest

There are no conflicts to declare.

Acknowledgements

This work was supported by the HBIS Group, China, and Australian Research Council (ARC) Linkage Project No. LP160101729. S. Garg received scholarship support from the University of Queensland Graduate School and the HBIS-UQ Innovation Centre for Sustainable Steel. A. Z. Weber acknowledges support for his effort on this review from the Joint Center for Artificial Photosynthesis, a DOE Energy Innovation Hub, supported through the Office of Science of the U.S. Department of Energy under Award No. DE-SC0004993.

References

1 H. Naims, *Environ. Sci. Pollut. Res.*, 2016, **23**, 22226–22241.
2 *Global CCS Institute, The Global Status of CCS: 2015, Summary Report*, Melbourne, Australia, 2015.
3 M. M. Halmann, *Chemical Fixation of Carbon DioxideMethods for Recycling CO2 into Useful Products*, CRC press, 1993.
4 A. Al-Mamoori, A. Krishnamurthy, A. A. Rownaghi and F. Rezaei, *Energy Technol.*, 2017, **5**, 834–849.
5 S. Chu and A. Majumdar, *Nature*, 2012, **488**, 294.
6 E. V. Kondratenko, G. Mul, J. Baltrusaitis, G. O. Larrazabal and J. Perez-Ramirez, *Energy Environ. Sci.*, 2013, **6**, 3112–3135.
7 H.-R. M. Jhong, S. Ma and P. J. A. Kenis, *Curr. Opin. Chem. Eng.*, 2013, **2**, 191–199.
8 A. S. Agarwal, Y. Zhai, D. Hill and N. Sridhar, *ChemSusChem*, 2011, **4**, 1301–1310.
9 O. S. Bushuyev, P. De Luna, C. T. Dinh, L. Tao, G. Saur, J. van de Lagemaat, S. O. Kelley and E. H. Sargent, *Joule*, 2018, **2**, 825–832.
10 D. R. Kauffman, J. Thakkar, R. Siva, C. Matranga, P. R. Ohodnicki, C. Zeng and R. Jin, *ACS Appl. Mater. Interfaces*, 2015, **7**, 15626–15632.
11 R. J. Lim, M. Xie, M. A. Sk, J.-M. Lee, A. Fisher, X. Wang and K. H. Lim, *Catal. Today*, 2014, **233**, 169–180.
12 N. Pardo and J. A. Moya, *Energy*, 2013, **54**, 113–128.
13 Opus-12, We have developed a device that recycles CO2 into chemicals and fuels, https://www.opus-12.com/technology.
14 C. E. R. Toronto, Technology,https://co2cert.com/technology/.
15 Evonik, Evonik and siemens to generate high-value specialty chemicals from carbon dioxide and eco-electricity, https://corporate.evonik.com/en/media/search/pages/news-details.aspx?NewsId=72457.
16 The Powerhaus Pavilion, http://greenangelenergy.ca/ph/mantraenergy.html, accessed at 1st December 2018.
17 E. Alper and O. Yuksel Orhan, *Petroleum*, 2017, **3**, 109–126.
18 Y. Hori, H. Konishi, T. Futamura, A. Murata, O. Koga, H. Sakurai and K. Oguma, *Electrochim. Acta*, 2005, **50**, 5354–5369.
19 A. Wuttig and Y. Surendranath, *ACS Catal.*, 2015, **5**, 4479–4484.
20 B. Jermann and J. Augustynski, *Electrochim. Acta*, 1994, **39**, 1891–1896.
21 G. Nogami, H. Itagaki and R. Shiratsuchi, *J. Electrochem. Soc.*, 1994, **141**, 1138–1142.
22 J. Yano, T. Morita, K. Shimano, Y. Nagami and S. Yamasaki, *J. Solid State Electrochem.*, 2007, **11**, 554–557.
23 J. Yano and S. Yamasaki, *J. Appl. Electrochem.*, 2008, **38**, 1721.
24 P. Kedzierzawski and J. Augustynski, *J. Electrochem. Soc.*, 1994, **141**, L58–L60.

25 B. Kumar, J. P. Brian, V. Atla, S. Kumari, K. A. Bertram, R. T. White and J. M. Spurgeon, *ACS Catal.*, 2016, **6**, 4739–4745.
26 L. M. Chiacchiarelli, Y. Zhai, G. S. Frankel, A. S. Agarwal and N. Sridhar, *J. Appl. Electrochem.*, 2012, **42**, 21–29.
27 J. Qiao, Y. Liu, F. Hong and J. Zhang, *Chem. Soc. Rev.*, 2014, **43**, 631–675.
28 D. Voiry, H. S. Shin, K. P. Loh and M. Chhowalla, *Nat. Rev. Chem.*, 2018, **2**, 0105.
29 Z. D. Dong, L. J. Long and Q. S. Zhang, *Adv. Mater. (Weinheim, Ger.)*, 2016, **28**, 3423–3452.
30 F. Li, D. R. MacFarlane and J. Zhang, *Nanoscale*, 2018, **10**, 6235–6260.
31 W. Yang, K. Dastafkan, C. Jia and C. Zhao, *Adv. Mater. Technol.*, 2018, 1700377.
32 Z. Sun, T. Ma, H. Tao, Q. Fan and B. Han, *Chem*, 2017, **3**, 560–587.
33 R. Francke, B. Schille and M. Roemelt, *Chem. Rev.*, 2018, **118**, 4631–4701.
34 T. Ziqi, P. Chad and C. Liang, *Adv. Theory Simul.*, 2018, **1**, 1800004.
35 C. W. Lee, K. D. Yang, D. H. Nam, J. H. Jang, N. H. Cho, S. W. Im and K. T. Nam, *Adv. Mater. (Weinheim, Ger.)*, 2018, 1704717.
36 K. A. Grice, *Coord. Chem. Rev.*, 2017, **336**, 78–95.
37 E. E. Benson, C. P. Kubiak, A. J. Sathrum and J. M. Smieja, *Chem. Soc. Rev.*, 2009, **38**, 89–99.
38 N. Kornienko, Y. Zhao, C. S. Kley, C. Zhu, D. Kim, S. Lin, C. J. Chang, O. M. Yaghi and P. Yang, *J. Am. Chem. Soc.*, 2015, **137**, 14129–14135.
39 D. M. Weekes, D. A. Salvatore, A. Reyes, A. Huang and C. P. Berlinguette, *Acc. Chem. Res.*, 2018, **51**, 910–918.
40 B. Endrődi, G. Bencsik, F. Darvas, R. Jones, K. Rajeshwar and C. Janáky, *Prog. Energy Combust. Sci.*, 2017, **62**, 133–154.
41 M. Bevilacqua, J. Filippi, H. A. Miller and F. Vizza, *Energy Technol.*, 2015, **3**, 197–210.
42 S. Ma, J. Liu, K. Sasaki, S. M. Lyth and P. J. A. Kenis, *Energy Technol.*, 2017, **5**, 861–863.
43 R. B. Kutz, Q. Chen, H. Yang, S. D. Sajjad, Z. Liu and I. R. Masel, *Energy Technol.*, 2017, **5**, 929–936.
44 D. Materials, CO_2 Electrolyzers, https://dioxidematerials.com/technology/co2-electrolysis/.
45 C.-T. Dinh, T. Burdyny, M. G. Kibria, A. Seifitokaldani, C. M. Gabardo, F. P. García de Arquer, A. Kiani, J. P. Edwards, P. De Luna, O. S. Bushuyev, C. Zou, R. Quintero-Bermudez, Y. Pang, D. Sinton and E. H. Sargent, *Science*, 2018, **360**, 783–787.
46 Skyre, Products: CO_2RENEWTM, https://www.skyre-inc.com/products/co2renew/.
47 T. Haas, R. Krause, R. Weber, M. Demler and G. Schmid, *Nat. Catal.*, 2018, **1**, 32–39.
48 J. Qiao, Y. Liu and J. Zhang, *Electrochemical Reduction of Carbon Dioxide: Fundamentals and Technologies*, CRC Press, Boca Raton, 2016.
49 A. J. Bard and L. R. Faulkner, *Electrochemical methods: fundamentals and applications*, Wiley, 1980.
50 K. Scott, in *Sustainable and Green Electrochemical Science and Technology*, 2017, pp. 27–85, DOI: 10.1002/9781118698075.ch2.
51 M. S. Faber, R. Dziedzic, M. A. Lukowski, N. S. Kaiser, Q. Ding and S. Jin, *J. Am. Chem. Soc.*, 2014, **136**, 10053–10061.
52 K. Zeng and D. Zhang, *Prog. Energy Combust. Sci.*, 2010, **36**, 307–326.
53 T. Burdyny and W. A. Smith, *Energy Environ. Sci.*, 2019, **12**, 1442–1453.
54 E. J. Dufek, T. E. Lister and M. E. McIlwain, *J. Appl. Electrochem.*, 2011, **41**, 623–631.
55 H. Hashiba, L.-C. Weng, Y. Chen, H. K. Sato, S. Yotsuhashi, C. Xiang and A. Z. Weber, *J. Phys. Chem. C*, 2018, **122**, 3719–3726.
56 N. Gupta, M. Gattrell and B. MacDougall, *J. Appl. Electrochem.*, 2006, **36**, 161–172.
57 P. Lobaccaro, M. R. Singh, E. L. Clark, Y. Kwon, A. T. Bell and J. W. Ager, *Phys. Chem. Chem. Phys.*, 2016, **18**, 26777–26785.
58 L.-C. Weng, A. T. Bell and A. Z. Weber, *Phys. Chem. Chem. Phys.*, 2018, **20**, 16973–16984.
59 D. Wakerley, S. Lamaison, F. Ozanam, N. Menguy, D. Mercier, P. Marcus, M. Fontecave and V. Mougel, *Nat. Mater.*, 2019, **18**, 1222–1227.
60 L. D. Chen, M. Urushihara, K. Chan and J. K. Nørskov, *ACS Catal.*, 2016, **6**, 7133–7139.
61 R. B. Sandberg, J. H. Montoya, K. Chan and J. K. Nørskov, *Surf. Sci.*, 2016, **654**, 56–62.
62 M. R. Singh, Y. Kwon, Y. Lum, J. W. Ager and A. T. Bell, *J. Am. Chem. Soc.*, 2016, **138**, 13006–13012.
63 J. Resasco, L. D. Chen, E. Clark, C. Tsai, C. Hahn, T. F. Jaramillo, K. Chan and A. T. Bell, *J. Am. Chem. Soc.*, 2017, **139**, 11277–11287.
64 A. S. Varela, W. Ju, T. Reier and P. Strasser, *ACS Catal.*, 2016, **6**, 2136–2144.
65 M. S. Xie, B. Y. Xia, Y. Li, Y. Yan, Y. Yang, Q. Sun, S. H. Chan, A. Fisher and X. Wang, *Energy Environ. Sci.*, 2016, **9**, 1687–1695.
66 D. Gao, F. Scholten and B. Roldan Cuenya, *ACS Catal.*, 2017, **7**, 5112–5120.
67 M. R. Singh, J. D. Goodpaster, A. Z. Weber, M. Head-Gordon and A. T. Bell, *Proc. Natl. Acad. Sci.*, 2017, **114**, E8812–E8821.
68 C. S. Chen, A. D. Handoko, J. H. Wan, L. Ma, D. Ren and B. S. Yeo, *Catal. Sci. Technol.*, 2015, **5**, 161–168.
69 D. T. Whipple and P. J. A. Kenis, *J. Phys. Chem. Lett.*, 2010, **1**, 3451–3458.
70 C. Delacourt, P. L. Ridgway and J. Newman, *J. Electrochem. Soc.*, 2010, **157**, B1902–B1910.
71 Y. C. Li, D. Zhou, Z. Yan, R. H. Gonçalves, D. A. Salvatore, C. P. Berlinguette and T. E. Mallouk, *ACS Energy Lett.*, 2016, **1**, 1149–1153.
72 M. R. Singh, K. Papadantonakis, C. Xiang and N. S. Lewis, *Energy Environ. Sci.*, 2015, **8**, 2760–2767.
73 C. Xiang, K. M. Papadantonakis and N. S. Lewis, *Mater. Horiz.*, 2016, **3**, 169–173.
74 X. Li and I. Sabir, *Int. J. Hydrogen Energy*, 2005, **30**, 359–371.

75 J. Wang and H. Wang, *Fuel Cells*, 2012, **12**, 989–1003.
76 P. J. Hamilton and B. G. Pollet, *Fuel Cells*, 2010, **10**, 489–509.
77 D. M. F. Santos, C. A. C. Sequeira and J. L. Figueiredo, *Quim. Nova*, 2013, **36**, 1176–1193.
78 F. Harnisch, U. Schröder and F. Scholz, *Environ. Sci. Technol.*, 2008, **42**, 1740–1746.
79 N. M. Vargas-Barbosa, G. M. Geise, M. A. Hickner and T. E. Mallouk, *ChemSusChem*, 2014, **7**, 3017–3020.
80 M. B. McDonald, J. P. Bruce, K. McEleney and M. S. Freund, *ChemSusChem*, 2015, **8**, 2645–2654.
81 J. Luo, D. A. Vermaas, D. Bi, A. Hagfeldt, W. A. Smith and M. Grätzel, *Adv. Energy Mater.*, 2016, **6**, 1600100.
82 M. B. McDonald, S. Ardo, N. S. Lewis and M. S. Freund, *ChemSusChem*, 2014, **7**, 3021–3027.
83 R. S. Reiter, W. White and S. Ardo, *J. Electrochem. Soc.*, 2016, **163**, H3132–H3134.
84 A. Kusoglu and A. Z. Weber, *Chem. Rev.*, 2017, **117**, 987–1104.
85 J. J. Kaczur, H. Yang, Z. Liu, S. D. Sajjad and R. I. Masel, *Front. Chem.*, 2018, **6**, 263.
86 T. Luo, S. Abdu and M. Wessling, *J. Membr. Sci.*, 2018, **555**, 429–454.
87 K. F. L. Hagesteijn, S. Jiang and B. P. Ladewig, *J. Mater. Sci.*, 2018, **53**, 11131–11150.
88 D. Y. Leung and J. Xuan, *Micro & nano-engineering of fuel cells*, Crc Press, 2015.
89 D. W. Dewulf and A. J. Bard, *Catal. Lett.*, 1988, **1**, 73–79.
90 C. Delacourt, P. L. Ridgway, J. B. Kerr and J. Newman, *J. Electrochem. Soc.*, 2008, **155**, B42–B49.
91 Y. Hori, H. Ito, K. Okano, K. Nagasu and S. Sato, *Electrochim. Acta*, 2003, **48**, 2651–2657.
92 N. Ziv and D. R. Dekel, *Electrochem. Commun.*, 2018, **88**, 109–113.
93 J. R. Varcoe, P. Atanassov, D. R. Dekel, A. M. Herring, M. A. Hickner, P. A. Kohl, A. R. Kucernak, W. E. Mustain, K. Nijmeijer, K. Scott, T. Xu and L. Zhuang, *Energy Environ. Sci.*, 2014, **7**, 3135–3191.
94 K. N. Grew, X. Ren and D. Chu, *Electrochem. Solid-State Lett.*, 2011, **14**, B127–B131.
95 Z. Sun, J. Pan, J. Guo and F. Yan, *Adv. Sci.*, 2018, **5**, 1800065.
96 J. Albo, A. Sáez, J. Solla-Gullón, V. Montiel and A. Irabien, *Appl. Catal., B*, 2015, **176**, 709–717.
97 M. Alvarez-Guerra, S. Quintanilla and A. Irabien, *Chem. Eng. J. (Lausanne)*, 2012, **207**, 278–284.
98 M. Ramdin, A. R. T. Morrison, M. de Groen, R. van Haperen, R. de Kler, L. J. P. van den Broeke, J. P. M. Trusler, W. de Jong and T. J. H. Vlugt, *Ind. Eng. Chem. Res.*, 2019, **58**, 1834–1847.
99 K. P. Kuhl, E. R. Cave, D. N. Abram and T. F. Jaramillo, *Energy Environ. Sci.*, 2012, **5**, 7050–7059.
100 T. Hatsukade, K. P. Kuhl, E. R. Cave, D. N. Abram and T. F. Jaramillo, *Phys. Chem. Chem. Phys.*, 2014, **16**, 13814–13819.
101 J. T. Feaster, C. Shi, E. R. Cave, T. Hatsukade, D. N. Abram, K. P. Kuhl, C. Hahn, J. K. Nørskov and T. F. Jaramillo, *ACS Catal.*, 2017, **7**, 4822–4827.
102 E. R. Cave, J. H. Montoya, K. P. Kuhl, D. N. Abram, T. Hatsukade, C. Shi, C. Hahn, J. K. Norskov and T. F. Jaramillo, *Phys. Chem. Chem. Phys.*, 2017, **19**, 15856–15863.
103 K. Manthiram, B. J. Beberwyck and A. P. Alivisatos, *J. Am. Chem. Soc.*, 2014, **136**, 13319–13325.
104 E. L. Clark, M. R. Singh, Y. Kwon and A. T. Bell, *Anal. Chem.*, 2015, **87**, 8013–8020.
105 J. Balster, D. F. Stamatialis and M. Wessling, *Chem. Eng. Process.*, 2004, **43**, 1115–1127.
106 J. Kamcev, R. Sujanani, E.-S. Jang, N. Yan, N. Moe, D. R. Paul and B. D. Freeman, *J. Membr. Sci.*, 2018, **547**, 123–133.
107 E. J. Dufek, T. E. Lister and M. E. McIlwain, *Electrochem. Solid-State Lett.*, 2012, **15**, B48–B50.
108 E. J. Dufek, T. E. Lister, S. G. Stone and M. E. McIlwain, *J. Electrochem. Soc.*, 2012, **159**, F514–F517.
109 K. Hara and T. Sakata, *Bull. Chem. Soc. Jpn.*, 1997, **70**, 571–576.
110 P. Jeanty, C. Scherer, E. Magori, K. Wiesner-Fleischer, O. Hinrichsen and M. Fleischer, *J. CO2 Util.*, 2018, **24**, 454–462.
111 D. Higgins, C. Hahn, C. Xiang, T. F. Jaramillo and A. Z. Weber, *ACS Energy Lett.*, 2019, **4**, 317–324.
112 W. Lee, Y. E. Kim, M. H. Youn, S. K. Jeong and K. T. Park, *Angew. Chem.*, 2018, **130**, 6999–7003.
113 I. Merino-Garcia, J. Albo and A. Irabien, *Nanotechnology*, 2017, **29**, 014001.
114 D. A. Salvatore, D. M. Weekes, J. He, K. E. Dettelbach, Y. C. Li, T. E. Mallouk and C. P. Berlinguette, *ACS Energy Lett.*, 2018, **3**, 149–154.
115 D. T. Whipple, E. C. Finke and P. J. A. Kenis, *Electrochem. Solid-State Lett.*, 2010, **13**, B109–B111.
116 R. S. Jayashree, S. K. Yoon, F. R. Brushett, P. O. Lopez-Montesinos, D. Natarajan, L. J. Markoski and P. J. A. Kenis, *J. Power Sources*, 2010, **195**, 3569–3578.
117 M. M. Morgan, L. Peter, L. Yanwei and W. A. Joel, *J. Phys. D: Appl. Phys.*, 2017, **50**, 154006.
118 S. Verma, B. Kim, H.-R. M. Jhong, S. Ma and P. J. A. Kenis, *ChemSusChem*, 2016, **9**, 1972–1979.
119 J. Spurgeon and B. Kumar, *Energy Environ. Sci.*, 2018, **11**, 1536–1551.
120 J. B. Greenblatt, D. J. Miller, J. W. Ager, F. A. Houle and I. D. Sharp, *Joule*, 2018, **2**, 381–420.
121 J. H. Lunsford, P. Qiu, M. P. Rosynek and Z. Yu, *J. Phys. Chem. B*, 1998, **102**, 167–173.
122 A. Elfasakhany, *Eng. Sci. Technol. Int J.*, 2015, **18**, 713–719.
123 P. Tian, Y. Wei, M. Ye and Z. Liu, *ACS Catal.*, 2015, **5**, 1922–1938.
124 S. Şahin, Ş. S. Bayazit, M. Bilgin and İ. İnci, *J. Chem. Eng. Data*, 2010, **55**, 1519–1522.
125 G. A. Olah, A. Goeppert and G. K. S. Prakash, *J. Org. Chem.*, 2009, **74**, 487–498.
126 H. S. Abdelkader, L. Touhami, B. M. Lakhdar, K. Abdellah, G. Toufik and B. B. Fouzi, *presented in part at the International Conference on Environmental*, Biomedical and Biotechnology Singapore, 2012.

127 H. Yang, J. J. Kaczur, S. D. Sajjad and R. I. Masel, *J. CO2 Util.*, 2017, **20**, 208–217.
128 H. S. Jeon, S. Kunze, F. Scholten and B. Roldan Cuenya, *ACS Catal.*, 2018, **8**, 531–535.
129 C. W. Lee, J. S. Hong, K. D. Yang, K. Jin, J. H. Lee, H.-Y. Ahn, H. Seo, N.-E. Sung and K. T. Nam, *ACS Catal.*, 2018, **8**, 931–937.
130 F. Li, L. Chen, M. Xue, T. Williams, Y. Zhang, D. R. MacFarlane and J. Zhang, *Nano Energy*, 2017, **31**, 270–277.
131 Y. Hori, H. Wakebe, T. Tsukamoto and O. Koga, *Electrochim. Acta*, 1994, **39**, 1833–1839.
132 Q. Lu, J. Rosen, Y. Zhou, G. S. Hutchings, Y. C. Kimmel, J. G. Chen and F. Jiao, *Nat. Commun.*, 2014, **5**, 3242.
133 S. Liu, J. Xiao, X. F. Lu, J. Wang, X. Wang and X. W. Lou, *Angew. Chem., Int. Ed.*, 2019, **58**, 8499–8503.
134 M. Rahaman, A. Dutta, A. Zanetti and P. Broekmann, *ACS Catal.*, 2017, **7**, 7946–7956.
135 Q. Li, J. Fu, W. Zhu, Z. Chen, B. Shen, L. Wu, Z. Xi, T. Wang, G. Lu, J.-j. Zhu and S. Sun, *J. Am. Chem. Soc.*, 2017, **139**, 4290–4293.
136 L. Dai, Q. Qin, P. Wang, X. Zhao, C. Hu, P. Liu, R. Qin, M. Chen, D. Ou, C. Xu, S. Mo, B. Wu, G. Fu, P. Zhang and N. Zheng, *Sci. Adv.*, 2017, **3**, e1701069.
137 P. Su, W. Xu, Y. Qiu, T. Zhang, X. Li and H. Zhang, *ChemSusChem*, 2018, **11**, 848–853.
138 H. Li and C. Oloman, *J. Appl. Electrochem.*, 2005, **35**, 955–965.
139 D. Kopljar, A. Inan, P. Vindayer, N. Wagner and E. Klemm, *J. Appl. Electrochem.*, 2014, **44**, 1107–1116.
140 Z. Bitar, A. Fecant, E. Trela-Baudot, S. Chardon-Noblat and D. Pasquier, *Appl. Catal., B*, 2016, **189**, 172–180.
141 M. Schwartz, R. L. Cook, V. M. Kehoe, R. C. MacDuff, J. Patel and A. F. Sammells, *J. Electrochem. Soc.*, 1993, **140**, 614–618.
142 M. N. Mahmood, D. Masheder and C. J. Harty, *J. Appl. Electrochem.*, 1987, **17**, 1159–1170.
143 G. K. S. Prakash, F. A. Viva and G. A. Olah, *J. Power Sources*, 2013, **223**, 68–73.
144 A. Del Castillo, M. Alvarez-Guerra, J. Solla-Gullón, A. Sáez, V. Montiel and A. Irabien, *J. CO2 Util.*, 2017, **18**, 222–228.
145 M. H. Shojaeefard, G. R. Molaeimanesh, M. Nazemian and M. R. Moqaddari, *Int. J. Hydrogen Energy*, 2016, **41**, 20276–20293.
146 A. Z. Weber, R. L. Borup, R. M. Darling, P. K. Das, T. J. Dursch, W. Gu, D. Harvey, A. Kusoglu, S. Litster, M. M. Mench, R. Mukundan, J. P. Owejan, J. G. Pharoah, M. Secanell and I. V. Zenyuk, *J. Electrochem. Soc.*, 2014, **161**, F1254–F1299.
147 D. M. Fadzillah, M. I. Rosli, M. Z. M. Talib, S. K. Kamarudin and W. R. W. Daud, *Renewable Sustainable Energy Rev.*, 2017, **77**, 1001–1009.
148 J. Lai, A. Nsabimana, R. Luque and G. Xu, *Joule*, 2018, **2**, 76–93.
149 F. C. Walsh, L. F. Arenas and C. Ponce de León, *J. Chem. Technol. Biotechnol.*, 2018, **93**, 3073–3090.
150 F. Lux, *J. Mater. Sci.*, 1993, **28**, 285–301.
151 L. I. Chernyshev and V. V. Skorokhod, *Powder Metall. Met. Ceram.*, 2003, **42**, 88–93.
152 B. I. Shklovskiĭ and A. L. Éfros, *Phys.-Usp.*, 1975, **18**, 845–862.
153 R. Lipton, *Proc. R. Soc. London, Ser. A*, 1998, **454**, 1371–1382.
154 Y. Lum, B. Yue, P. Lobaccaro, A. T. Bell and J. W. Ager, *J. Phys. Chem. C*, 2017, **121**, 14191–14203.
155 M. Ma, B. J. Trześniewski, J. Xie and W. A. Smith, *Angew. Chem., Int. Ed.*, 2016, **55**, 9748–9752.
156 H. Yano, F. Shirai, M. Nakayama and K. Ogura, *J. Electroanal. Chem.*, 2002, **519**, 93–100.
157 R. L. Cook, R. C. MacDuff and A. F. Sammells, *J. Electrochem. Soc.*, 1990, **137**, 607–608.
158 K. Hara and T. Sakata, *J. Electrochem. Soc.*, 1997, **144**, 539–545.
159 K. Hara, A. Kudo, T. Sakata and M. Watanabe, *J. Electrochem. Soc.*, 1995, **142**, L57–L59.
160 Q. Wang, H. Dong and H. Yu, *J. Power Sources*, 2014, **271**, 278–284.
161 S. Park, J.-W. Lee and B. N. Popov, *Int. J. Hydrogen Energy*, 2012, **37**, 5850–5865.
162 B. Kim, F. Hillman, M. Ariyoshi, S. Fujikawa and P. J. A. Kenis, *J. Power Sources*, 2016, **312**, 192–198.
163 A. Del Castillo, M. Alvarez-Guerra and A. Irabien, *AIChE J.*, 2014, **60**, 3557–3564.
164 S. Ikeda, T. Ito, K. Azuma, K. Ito and H. Noda, *Denki Kagaku*, 1995, **63**, 303–309.
165 J. Albo and A. Irabien, *J. Catal.*, 2016, **343**, 232–239.
166 B. C. Marepally, C. Ampelli, C. Genovese, T. Saboo, S. Perathoner, F. M. Wisser, L. Veyre, J. Canivet, E. A. Quadrelli and G. Centi, *ChemSusChem*, 2017, **10**, 4442–4446.
167 E. Irtem, T. Andreu, A. Parra, M. D. Hernández-Alonso, S. García-Rodríguez, J. M. Riesco-García, G. Penelas-Pérez and J. R. Morante, *J. Mater. Chem. A*, 2016, **4**, 13582–13588.
168 Q. Wang, X. Wang, C. Wu, Y. Cheng, Q. Sun, H. Dong and H. Yu, *Sci. Rep.*, 2017, **7**, 13711.
169 Q. Wang, H. Dong, H. Yu and H. Yu, *J. Power Sources*, 2015, **279**, 1–5.
170 S. Guan, A. Agarwal, E. Rode, D. Hill and N. Sridhar, *Advances in Materials Science for Environmental and Energy Technologies II: Ceramic Transactions*, 2013, vol. 241, pp. 231–243.
171 D. Masheder and K. P. J. Williams, *J. Raman Spectrosc.*, 1987, **18**, 387–390.
172 L. Cindrella, A. M. Kannan, J. F. Lin, K. Saminathan, Y. Ho, C. W. Lin and J. Wertz, *J. Power Sources*, 2009, **194**, 146–160.
173 J. Park, H. Oh, T. Ha, Y. I. Lee and K. Min, *Appl. Energy*, 2015, **155**, 866–880.
174 L. Han, W. Zhou and C. Xiang, *ACS Energy Lett.*, 2018, **3**, 855–860.
175 D. Kopljar, N. Wagner and E. Klemm, *Chem. Eng. Technol.*, 2016, **39**, 2042–2050.
176 Q. Wang, H. Dong and H. Yu, *RSC Adv.*, 2014, **4**, 59970–59976.

177 T. Van Nguyen, A. Ahosseini, X. Wang, V. Yarlagadda, A. Kwong, A. Z. Weber, P. Deevanhxay, S. Tsushima and S. Hirai, *J. Electrochem. Soc.*, 2015, **162**, F1451–F1460.
178 R. Omrani and B. Shabani, *Int. J. Hydrogen Energy*, 2017, **42**, 28515–28536.
179 J. Wu, F. G. Risalvato, S. Ma and X.-D. Zhou, *J. Mater. Chem. A*, 2014, **2**, 1647–1651.
180 A. Li, H. Wang, J. Han and L. Liu, *Front. Chem. Sci. Eng.*, 2012, **6**, 381–388.
181 T.-J. Park, S. Banerjee, T. Hemraj-Benny and S. S. Wong, *J. Mater. Chem.*, 2006, **16**, 141–154.
182 M. Pumera, A. Ambrosi and E. L. K. Chng, *Chem. Sci.*, 2012, **3**, 3347–3355.
183 C. M. Long, M. A. Nascarella and P. A. Valberg, *Environ. Pollut.*, 2013, **181**, 271–286.
184 A. Z. Weber and J. Newman, *J. Electrochem. Soc.*, 2005, **152**, A677–A688.
185 M. Prasanna, H. Y. Ha, E. A. Cho, S. A. Hong and I. H. Oh, *J. Power Sources*, 2004, **131**, 147–154.
186 T. Turek, I. Moussallem, A. Bulan, N. Schmitz and P. Weuta, European Patent Office, EP2397578A2, 2016.
187 Y. Wang, J. Liu, Y. Wang, A. M. Al-Enizi and G. Zheng, *Small*, 2017, **13**, 1701809.
188 J. He, N. J. J. Johnson, A. Huang and C. P. Berlinguette, *ChemSusChem*, 2018, **11**, 48–57.
189 L.-C. Weng, A. T. Bell and A. Z. Weber, *Energy Environ. Sci.*, 2019, **12**, 1950–1968.
190 H. Mistry, F. Behafarid, R. Reske, A. S. Varela, P. Strasser and B. Roldan Cuenya, *ACS Catal.*, 2016, **6**, 1075–1080.
191 B. A. Rosen, A. Salehi-Khojin, M. R. Thorson, W. Zhu, D. T. Whipple, P. J. A. Kenis and R. I. Masel, *Science*, 2011, **334**, 643–644.
192 H. Yang, J. J. Kaczur, S. D. Sajjad and R. I. Masel, *ECS Trans.*, 2017, **77**, 1425–1431.
193 H. R. M. Jhong, F. R. Brushett and P. J. A. Kenis, *Adv. Energy Mater.*, 2013, **3**, 589–599.
194 K. Nakata, T. Ozaki, C. Terashima, A. Fujishima and Y. Einaga, *Angew. Chem.*, 2014, **126**, 890–893.
195 P. P. Sharma and X. D. Zhou, *Wiley Interdiscip. Rev.: Energy Environ.*, 2017, **6**, e239.
196 W. Plieth, in *Electrochemistry for Materials Science*, Elsevier, Amsterdam, 2008, pp. 1–26, DOI: 10.1016/B978-044452792-9.50003-8.
197 X. Lu, D. Y. C. Leung, H. Wang, M. K. H. Leung and J. Xuan, *ChemElectroChem*, 2014, **1**, 836–849.
198 J.-P. Jones, G. K. S. Prakash and G. A. Olah, *Isr. J. Chem.*, 2014, **54**, 1451–1466.
199 B. M. Setterfield-Price and R. A. W. Dryfe, *J. Electroanal. Chem.*, 2014, **730**, 48–58.
200 E. L. Clark, J. Resasco, A. Landers, J. Lin, L.-T. Chung, A. Walton, C. Hahn, T. F. Jaramillo and A. T. Bell, *ACS Catal.*, 2018, **8**, 6560–6570.
201 Á. Pérez-Salado Kamps, E. Meyer, B. Rumpf and G. Maurer, *J. Chem. Eng. Data*, 2007, **52**, 817–832.
202 Y. Liu, M. Hou, G. Yang and B. Han, *J. Supercrit. Fluids*, 2011, **56**, 125–129.
203 D. Tong, J. P. M. Trusler, G. C. Maitland, J. Gibbins and P. S. Fennell, *Int. J. Greenhouse Gas Control*, 2012, **6**, 37–47.
204 M. Wagner, I. von Harbou, J. Kim, I. Ermatchkova, G. Maurer and H. Hasse, *J. Chem. Eng. Data*, 2013, **58**, 883–895.
205 W. Lv, R. Zhang, P. Gao and L. Lei, *J. Power Sources*, 2014, **253**, 276–281.
206 W. Lv, J. Zhou, F. Kong, H. Fang and W. Wang, *Int. J. Hydrogen Energy*, 2016, **41**, 1585–1591.
207 F. Cai, D. Gao, H. Zhou, G. Wang, T. He, H. Gong, S. Miao, F. Yang, J. Wang and X. Bao, *Chem. Sci.*, 2017, **8**, 2569–2573.
208 A. L. Kohl, R. Nielsen and A. L. Kohl, *Gas purification*, Gulf Pub., Houston, Tex, 5th edn, 1997.
209 Y. Hori, K. Katsuhei, A. Murata and S. Suzuki, *Chem. Lett.*, 1986, **15**, 897–898.
210 K. Hara, A. Kudo and T. Sakata, *J. Electroanal. Chem.*, 1995, **391**, 141–147.
211 M. Jitaru, D. A. Lowy, M. Toma, B. C. Toma and L. Oniciu, *J. Appl. Electrochem.*, 1997, **27**, 875–889.
212 M. Todoroki, K. Hara, A. Kudo and T. Sakata, *J. Electroanal. Chem.*, 1995, **394**, 199–203.
213 D. Ren, Y. Deng, A. D. Handoko, C. S. Chen, S. Malkhandi and B. S. Yeo, *ACS Catal.*, 2015, **5**, 2814–2821.
214 D. Raciti, K. J. Livi and C. Wang, *Nano Lett.*, 2015, **15**, 6829–6835.
215 A. Bandi, M. Specht, T. Weimer and K. Schaber, *Energy Convers. Manage.*, 1995, **36**, 899–902.
216 M. Gattrell, N. Gupta and A. Co, *Energy Convers. Manage.*, 2007, **48**, 1255–1265.
217 S. Stucki, A. Schuler and M. Constantinescu, *Int. J. Hydrogen Energy*, 1995, **20**, 653–663.
218 K. Hara, A. Tsuneto, A. Kudo and T. Sakata, *J. Electroanal. Chem.*, 1997, **434**, 239–243.
219 P. Dubé and G. M. Brisard, *J. Electroanal. Chem.*, 2005, **582**, 230–240.
220 K. Ogura, *J. CO2 Util.*, 2013, **1**, 43–49.
221 K. Ogura and M. D. Salazar-Villalpando, *JOM*, 2011, **63**, 35–38.
222 M. Ma, K. Djanashvili and W. A. Smith, *Angew. Chem., Int. Ed.*, 2016, **55**, 6680–6684.
223 A. Murata and Y. Hori, *Bull. Chem. Soc. Jpn.*, 1991, **64**, 123–127.
224 M. R. Thorson, K. I. Siil and P. J. A. Kenis, *J. Electrochem. Soc.*, 2013, **160**, F69–F74.
225 S. Verma, X. Lu, S. Ma, R. I. Masel and P. J. A. Kenis, *Phys. Chem. Chem. Phys.*, 2016, **18**, 7075–7084.
226 W. Paik, T. N. Andersen and H. Eyring, *Electrochim. Acta*, 1969, **14**, 1217–1232.
227 H. Yoshio and S. Shin, *Bull. Chem. Soc. Jpn.*, 1982, **55**, 660–665.
228 S. Ringe, E. L. Clark, J. Resasco, A. Walton, B. Seger, A. T. Bell and K. Chan, *Energy Environ. Sci.*, 2019, **12**, 3001–3014.
229 Y. Hori, in *Modern Aspects of Electrochemistry*, ed. C. G. Vayenas, R. E. White and M. E. Gamboa-Aldeco, Springer, New York, New York, NY, 2008, pp. 89–189, DOI: 10.1007/978-0-387-49489-0_3.

230 M. E. Essington, *Soil and water chemistry: an integrative approach*, CRC Press, 2015.
231 A. N. Frumkin, *Trans. Faraday Soc.*, 1959, **55**, 156–167.
232 H. Kim, H. S. Park, Y. J. Hwang and B. K. Min, *J. Phys. Chem. C*, 2017, **121**, 22637–22643.
233 M. Liu, Y. Pang, B. Zhang, P. De Luna, O. Voznyy, J. Xu, X. Zheng, C. T. Dinh, F. Fan, C. Cao, F. P. G. de Arquer, T. S. Safaei, A. Mepham, A. Klinkova, E. Kumacheva, T. Filleter, D. Sinton, S. O. Kelley and E. H. Sargent, *Nature*, 2016, **537**, 382.
234 J. N. Mills, I. T. McCrum and M. J. Janik, *Phys. Chem. Chem. Phys.*, 2014, **16**, 13699–13707.
235 D. Strmcnik, K. Kodama, D. van der Vliet, J. Greeley, V. R. Stamenkovic and N. M. Marković, *Nature Chem.*, 2009, **1**, 466.
236 E. Pérez-Gallent, G. Marcandalli, M. C. Figueiredo, F. Calle-Vallejo and M. T. M. Koper, *J. Am. Chem. Soc.*, 2017, **139**, 16412–16419.
237 A. Schizodimou and G. Kyriacou, *Electrochim. Acta*, 2012, **78**, 171–176.
238 Y. Hori, A. Murata and R. Takahashi, *J. Chem. Soc., Faraday Trans. 1*, 1989, **85**, 2309–2326.
239 Y. Hori, in *Handbook of Fuel Cells*, John Wiley & Sons, Ltd, 2010, DOI: 10.1002/9780470974001.f207055.
240 J. Resasco, Y. Lum, E. Clark, J. Z. Zeledon and A. T. Bell, *ChemElectroChem*, 2018, **5**, 1064.
241 Y. Hori, A. Murata, R. Takahashi and S. Suzuki, *J. Chem. Soc., Chem. Commun.*, 1988, 17–19, DOI: 10.1039/C39880000017.
242 A. Wuttig, Y. Yoon, J. Ryu and Y. Surendranath, *J. Am. Chem. Soc.*, 2017, **139**, 17109–17113.
243 T. Cheng, H. Xiao and W. A. Goddard, *J. Am. Chem. Soc.*, 2016, **138**, 13802–13805.
244 A. Wuttig, M. Yaguchi, K. Motobayashi, M. Osawa and Y. Surendranath, *Proc. Natl. Acad. Sci.*, 2016, **113**, E4585–E4593.
245 H. Yano, T. Tanaka, M. Nakayama and K. Ogura, *J. Electroanal. Chem.*, 2004, **565**, 287–293.
246 K. Ogura, J. R. Ferrell, A. V. Cugini, E. S. Smotkin and M. D. Salazar-Villalpando, *Electrochim. Acta*, 2010, **56**, 381–386.
247 F. S. Roberts, K. P. Kuhl and A. Nilsson, *Angew. Chem., Int. Ed.*, 2015, **54**, 5179–5182.
248 Y. Kwon, Y. Lum, E. L. Clark, J. W. Ager and A. T. Bell, *ChemElectroChem*, 2016, **3**, 1012–1019.
249 S. Lee, D. Kim and J. Lee, *Angew. Chem.*, 2015, **127**, 14914–14918.
250 I. Shoichiro, T. Takehiko and I. Kaname, *Bull. Chem. Soc. Jpn.*, 1987, **60**, 2517–2522.
251 C. Amatore and J. M. Saveant, *J. Am. Chem. Soc.*, 1981, **103**, 5021–5023.
252 Y. B. Vassiliev, V. S. Bagotsky, N. V. Osetrova, O. A. Khazova and N. A. Mayorova, *J. Electroanal. Chem. Interfacial Electrochem.*, 1985, **189**, 271–294.
253 Y. Matsubara, *ACS Energy Lett.*, 2017, **2**, 1886–1891.
254 Y. Tomita, S. Teruya, O. Koga and Y. Hori, *J. Electrochem. Soc.*, 2000, **147**, 4164–4167.
255 O. Aschenbrenner and P. Styring, *Energy Environ. Sci.*, 2010, **3**, 1106–1113.
256 B. P. Sullivan, K. Krist and H. Guard, *Electrochemical and electrocatalytic reactions of carbon dioxide*, Elsevier, 2012.
257 S.-B. Park, C.-S. Shim, H. Lee and K.-H. Lee, *Fluid Phase Equilib.*, 1997, **134**, 141–149.
258 Y. Qiu, H. Zhong, W. Xu, T. Zhang, X. Li and H. Zhang, *J. Mater. Chem. A*, 2019, **7**, 5453–5462.
259 F.-Y. Jou, A. E. Mather and F. D. Otto, *Can. J. Chem. Eng.*, 1995, **73**, 140–147.
260 L. L. Snuffin, L. W. Whaley and L. Yu, *J. Electrochem. Soc.*, 2011, **158**, F155–F158.
261 S. Kaneco, K. Iiba, H. Katsumata, T. Suzuki and K. Ohta, *Electrochim. Acta*, 2006, **51**, 4880–4885.
262 S. Kaneco, K. Iiba, N.-h. Hiei, K. Ohta, T. Mizuno and T. Suzuki, *Electrochim. Acta*, 1999, **44**, 4701–4706.
263 T. Mizuno, A. Naitoh and K. Ohta, *J. Electroanal. Chem.*, 1995, **391**, 199–201.
264 E. D. Bates, R. D. Mayton, I. Ntai and J. H. Davis, *J. Am. Chem. Soc.*, 2002, **124**, 926–927.
265 J. L. Anderson, J. K. Dixon and J. F. Brennecke, *Acc. Chem. Res.*, 2007, **40**, 1208–1216.
266 J. F. Brennecke and B. E. Gurkan, *J. Phys. Chem. Lett.*, 2010, **1**, 3459–3464.
267 D. R. MacFarlane, N. Tachikawa, M. Forsyth, J. M. Pringle, P. C. Howlett, G. D. Elliott, J. H. Davis, M. Watanabe, P. Simon and C. A. Angell, *Energy Environ. Sci.*, 2014, **7**, 232–250.
268 M. V. Fedorov and A. A. Kornyshev, *Chem. Rev.*, 2014, **114**, 2978–3036.
269 M. Smiglak, J. Pringle, X. Lu, L. Han, S. Zhang, H. Gao, D. MacFarlane and R. Rogers, *Chem. Commun.*, 2014, **50**, 9228–9250.
270 M. Armand, F. Endres, D. R. MacFarlane, H. Ohno and B. Scrosati, *Nat. Mater.*, 2009, **8**, 621.
271 F. Zhou, S. Liu, B. Yang, P. Wang, A. S. Alshammari and Y. Deng, *Electrochem. Commun.*, 2014, **46**, 103–106.
272 M. Alvarez-Guerra, J. Albo, E. Alvarez-Guerra and A. Irabien, *Energy Environ. Sci.*, 2015, **8**, 2574–2599.
273 B. A. Rosen, J. L. Haan, P. Mukherjee, B. Braunschweig, W. Zhu, A. Salehi-Khojin, D. D. Dlott and R. I. Masel, *J. Phys. Chem. C*, 2012, **116**, 15307–15312.
274 B. A. Rosen, W. Zhu, G. Kaul, A. Salehi-Khojin and R. I. Masel, *J. Electrochem. Soc.*, 2013, **160**, H138–H141.
275 M. Asadi, B. Kumar, A. Behranginia, B. A. Rosen, A. Baskin, N. Repnin, D. Pisasale, P. Phillips, W. Zhu, R. Haasch, R. F. Klie, P. Král, J. Abiade and A. Salehi-Khojin, *Nat. Commun.*, 2014, **5**, 4470.
276 D. Niu, H. Wang, H. Li, Z. Wu and X. Zhang, *Electrochim. Acta*, 2015, **158**, 138–142.
277 L. Sun, G. K. Ramesha, P. V. Kamat and J. F. Brennecke, *Langmuir*, 2014, **30**, 6302–6308.
278 A. Salehi-Khojin, H.-R. M. Jhong, B. A. Rosen, W. Zhu, S. Ma, P. J. A. Kenis and R. I. Masel, *J. Phys. Chem. C*, 2013, **117**, 1627–1632.
279 J. L. DiMeglio and J. Rosenthal, *J. Am. Chem. Soc.*, 2013, **135**, 8798–8801.

280 J. Medina-Ramos, J. L. DiMeglio and J. Rosenthal, *J. Am. Chem. Soc.*, 2014, **136**, 8361–8367.
281 C. Costentin, M. Robert and J.-M. Saveant, *Chem. Soc. Rev.*, 2013, **42**, 2423–2436.
282 G. P. S. Lau, M. Schreier, D. Vasilyev, R. Scopelliti, M. Grätzel and P. J. Dyson, *J. Am. Chem. Soc.*, 2016, **138**, 7820–7823.
283 X. Zhang, Y. Zhao, S. Hu, M. E. Gliege, Y. Liu, R. Liu, L. Scudiero, Y. Hu and S. Ha, *Electrochim. Acta*, 2017, **247**, 281–287.
284 Q. Wang, C. Chen, J. Zhong, B. Zhang and Z. Cheng, *Aust. J. Chem.*, 2017, **70**, 293–300.
285 Q. Zhu, J. Ma, X. Kang, X. Sun, H. Liu, J. Hu, Z. Liu and B. Han, *Angew. Chem., Int. Ed.*, 2016, **55**, 9012–9016.
286 I. Ganesh, *Renewable Sustainable Energy Rev.*, 2014, **31**, 221–257.
287 A. S. Varela, M. Kroschel, T. Reier and P. Strasser, *Catal. Today*, 2016, **260**, 8–13.
288 R. Kas, R. Kortlever, H. Yılmaz, M. T. M. Koper and G. Mul, *ChemElectroChem*, 2015, **2**, 354–358.
289 I. Katsounaros, J. C. Meier, S. O. Klemm, A. A. Topalov, P. U. Biedermann, M. Auinger and K. J. J. Mayrhofer, *Electrochem. Commun.*, 2011, **13**, 634–637.
290 M. R. Singh, E. L. Clark and A. T. Bell, *Phys. Chem. Chem. Phys.*, 2015, **17**, 18924–18936.
291 A. S. Hall, Y. Yoon, A. Wuttig and Y. Surendranath, *J. Am. Chem. Soc.*, 2015, **137**, 14834–14837.
292 H. Hashiba, H. K. Sato, S. Yotsuhashi, K. Fujii, M. Sugiyama and Y. Nakano, *Sustainable Energy Fuels*, 2017, **1**, 1734–1739.
293 M. Gattrell, N. Gupta and A. Co, *J. Electroanal. Chem.*, 2006, **594**, 1–19.
294 L. Wang, S. A. Nitopi, E. Bertheussen, M. Orazov, C. G. Morales-Guio, X. Liu, D. C. Higgins, K. Chan, J. K. Nørskov, C. Hahn and T. F. Jaramillo, *ACS Catal.*, 2018, **8**, 7445–7454.
295 H. Ooka, M. C. Figueiredo and M. T. M. Koper, *Langmuir*, 2017, **33**, 9307–9313.
296 D. Strmcnik, M. Uchimura, C. Wang, R. Subbaraman, N. Danilovic, D. van der Vliet, A. P. Paulikas, V. R. Stamenkovic and N. M. Markovic, *Nat. Chem.*, 2013, **5**, 300.
297 J. Zheng, W. Sheng, Z. Zhuang, B. Xu and Y. Yan, *Sci. Adv.*, 2016, **2**, e1501602.
298 Y. Hori, A. Murata, R. Takahashi and S. Suzuki, *J. Am. Chem. Soc.*, 1987, **109**, 5022–5023.
299 Y. Hori, I. Takahashi, O. Koga and N. Hoshi, *J. Phys. Chem. B*, 2002, **106**, 15–17.
300 J. H. Montoya, C. Shi, K. Chan and J. K. Nørskov, *J. Phys. Chem. Lett.*, 2015, **6**, 2032–2037.
301 K. Jiang, R. B. Sandberg, A. J. Akey, X. Liu, D. C. Bell, J. K. Nørskov, K. Chan and H. Wang, *Nat. Catal.*, 2018, **1**, 111–119.
302 J. D. Goodpaster, A. T. Bell and M. Head-Gordon, *J. Phys. Chem. Lett.*, 2016, **7**, 1471–1477.
303 N. Hidetomo, I. Shoichiro, O. Yoshiyuki and I. Kaname, *Chem. Lett.*, 1989, **18**, 289–292.
304 K. W. Frese Jr, in *Electrochemical and Electrocatalytic Reactions of Carbon Dioxide*, ed. B. P. Sullivan, K. Krist and H. E. Guard, Elsevier, Amsterdam, 1993, pp. 145–216, DOI: 10.1016/B978-0-444-88316-2.50010-3.
305 J. J. Kim, D. P. Summers and K. W. Frese, *J. Electroanal. Chem. Interfacial Electrochem.*, 1988, **245**, 223–244.
306 Y. Hori, R. Takahashi, Y. Yoshinami and A. Murata, *J. Phys. Chem. B*, 1997, **101**, 7075–7081.
307 K. J. P. Schouten, Y. Kwon, C. J. M. van der Ham, Z. Qin and M. T. M. Koper, *Chem. Sci.*, 2011, **2**, 1902–1909.
308 K. J. P. Schouten, E. Pérez Gallent and M. T. M. Koper, *J. Electroanal. Chem.*, 2014, **716**, 53–57.
309 F. Calle-Vallejo and M. T. M. Koper, *Angew. Chem., Int. Ed.*, 2013, **52**, 7282–7285.
310 K. J. P. Schouten, Z. Qin, E. Pérez Gallent and M. T. M. Koper, *J. Am. Chem. Soc.*, 2012, **134**, 9864–9867.
311 J. O. M. Bockris and N. Pentland, *Trans. Faraday Soc.*, 1952, **48**, 833–839.
312 M. Jouny, W. Luc and F. Jiao, *Nat. Catal.*, 2018, **1**, 748–755.
313 M. Dunwell, X. Yang, B. P. Setzler, J. Anibal, Y. Yan and B. Xu, *ACS Catal.*, 2018, **8**, 3999–4008.
314 D. Raciti, M. Mao and C. Wang, *Nanotechnology*, 2017, **29**, 044001.
315 A. D. Handoko, C. W. Ong, Y. Huang, Z. G. Lee, L. Lin, G. B. Panetti and B. S. Yeo, *J. Phys. Chem. C*, 2016, **120**, 20058–20067.
316 X. Liu, P. Schlexer, J. Xiao, Y. Ji, L. Wang, R. B. Sandberg, M. Tang, K. S. Brown, H. Peng, S. Ringe, C. Hahn, T. F. Jaramillo, J. K. Nørskov and K. Chan, *Nat. Commun.*, 2019, **10**, 32.
317 Y. Y. Birdja and M. T. M. Koper, *J. Am. Chem. Soc.*, 2017, **139**, 2030–2034.
318 A. J. Garza, A. T. Bell and M. Head-Gordon, *ACS Catal.*, 2018, **8**, 1490–1499.
319 C. F. C. Lim, D. A. Harrington and A. T. Marshall, *Electrochim. Acta*, 2017, **238**, 56–63.
320 J. F. Richardson, J. H. Harker and J. R. Backhurst, *Coulson & Richardson's Chemical Engineering*, Butterworth-Heinemann London, 2002.
321 G. T. Rochelle, *Science*, 2009, **325**, 1652–1654.
322 F. Karadas, B. Köz, J. Jacquemin, E. Deniz, D. Rooney, J. Thompson, C. T. Yavuz, M. Khraisheh, S. Aparicio and M. Atihan, *Fluid Phase Equilib.*, 2013, **351**, 74–86.
323 P. Singh, D. W. F. Brilman and M. J. Groeneveld, *Int. J. Greenhouse Gas Control*, 2011, **5**, 61–68.
324 T. Mizuno, K. Ohta, A. Sasaki, T. Akai, M. Hirano and A. Kawabe, *Energy Sources*, 1995, **17**, 503–508.
325 S. Nakagawa, A. Kudo, M. Azuma and T. Sakata, *J. Electroanal. Chem. Interfacial Electrochem.*, 1991, **308**, 339–343.
326 H. De Jesús-Cardona, C. del Moral and C. R. Cabrera, *J. Electroanal. Chem.*, 2001, **513**, 45–51.
327 K. Hara, A. Kudo and T. Sakata, *J. Electroanal. Chem.*, 1997, **421**, 1–4.
328 K. Hara, A. Kudo and T. Sakata, *J. Electroanal. Chem.*, 1995, **386**, 257–260.

329 N. Sonoyama, M. Kirii and T. Sakata, *Electrochem. Commun.*, 1999, **1**, 213–216.
330 K. Hara, A. Tsuneto, A. Kudo and T. Sakata, *J. Electrochem. Soc.*, 1994, **141**, 2097–2103.
331 A. Kudo, S. Nakagawa, A. Tsuneto and T. Sakata, *J. Electrochem. Soc.*, 1993, **140**, 1541–1545.
332 E. Stránská and D. Neděla, *J. Ind. Text.*, 2018, **48**, 432–447.
333 F. L. Smith and A. H. Harvey, *Chem. Eng. Prog.*, 2007, **103**, 33–39.
334 J. H. Perry, *Chemical engineers' handbook*, ACS Publications, 1950.
335 M. J. Moran, H. N. Shapiro, D. D. Boettner and M. B. Bailey, *Fundamentals of engineering thermodynamics*, John Wiley & Sons, 2010.
336 J. Ryu, T. N. Andersen and H. Eyring, *J. Phys. Chem.*, 1972, **76**, 3278–3286.
337 J. Kestin, M. Sokolov and W. A. Wakeham, *J. Phys. Chem. Ref. Data*, 1978, **7**, 941–948.
338 E. N. Fuller, P. D. Schettler and J. C. Giddings, *Ind. Eng. Chem.*, 1966, **58**, 18–27.
339 J. J. Carroll, F.-Y. Jou, A. E. Mather and F. D. Otto, *Can. J. Chem. Eng.*, 1998, **76**, 945–951.
340 J. E. Davis and J. J. McKetta, *J. Chem. Eng. Data*, 1960, **5**, 374–375.
341 M. Azuma, K. Hashimoto, M. Hiramoto, M. Watanabe and T. Sakata, *J. Electroanal. Chem. Interfacial Electrochem.*, 1989, **260**, 441–445.
342 M. Azuma, K. Hashimoto, M. Hiramoto, M. Watanabe and T. Sakata, *J. Electrochem. Soc.*, 1990, **137**, 1772–1778.
343 S. T. Ahn, I. Abu-Baker and G. T. R. Palmore, *Catal. Today*, 2017, **288**, 24–29.
344 S. Kaneco, N.-h. Hiei, Y. Xing, H. Katsumata, H. Ohnishi, T. Suzuki and K. Ohta, *Electrochim. Acta*, 2002, **48**, 51–55.
345 J. Hussain, H. Jónsson and E. Skúlason, *ACS Catal.*, 2018, **8**, 5240–5249.
346 W. Luo, X. Nie, M. J. Janik and A. Asthagiri, *ACS Catal.*, 2016, **6**, 219–229.
347 Sustainion®Anion Exchange Membranes, https://dioxidematerials.com/technology/sustainion-membranes/, accessed 15/08/2019, 2019.
348 K. Scott, C. Xu and X. Wu, *Wiley Interdiscip. Rev.: Energy Environ.*, 2014, **3**, 24–41.
349 I. Vincent and D. Bessarabov, *Renewable Sustainable Energy Rev.*, 2018, **81**, 1690–1704.
350 F. Proietto, B. Schiavo, A. Galia and O. Scialdone, *Electrochim. Acta*, 2018, **277**, 30–40.
351 S. J. Davis, N. S. Lewis, M. Shaner, S. Aggarwal, D. Arent, I. L. Azevedo, S. M. Benson, T. Bradley, J. Brouwer, Y.-M. Chiang, C. T. M. Clack, A. Cohen, S. Doig, J. Edmonds, P. Fennell, C. B. Field, B. Hannegan, B.-M. Hodge, M. I. Hoffert, E. Ingersoll, P. Jaramillo, K. S. Lackner, K. J. Mach, M. Mastrandrea, J. Ogden, P. F. Peterson, D. L. Sanchez, D. Sperling, J. Stagner, J. E. Trancik, C.-J. Yang and K. Caldeira, *Science*, 2018, 360.
352 J. R. Hudkins, D. G. Wheeler, B. Pena and C. P. Berlinguette, *Energy Environ. Sci.*, 2016, **9**, 3417–3423.
353 S. Sabatino, A. Galia, G. Saracco and O. Scialdone, *ChemElectroChem*, 2017, **4**, 150–159.
354 T. E. Lister and E. J. Dufek, *Energy Fuels*, 2013, **27**, 4244–4249.
355 I. Moussallem, J. Jörissen, U. Kunz, S. Pinnow and T. Turek, *J. Appl. Electrochem.*, 2008, **38**, 1177–1194.